

9. JOINING

A. Forming Limits of Weld Metal in Aluminum Alloys and Advanced High-Strength Steels

Principal Investigator: Richard W. Davies

Pacific Northwest National Laboratory

P.O. Box 999, Richland, WA 99352-0999

(509) 375-6474; fax: (509) 375-5994; e-mail: rich.davies@pnl.gov

Technology Area Development Manager: Joseph A. Carpenter

(202) 586-1022; fax: (202) 586-1600; e-mail: joseph.carpenter@ee.doe.gov

Field Technical Manager: Mark T. Smith

(509) 375-4478; fax: (509) 375-4448; e-mail: mark.smith@pnl.gov

Participants: Elizabeth V. Stephens and Glenn J. Grant

Pacific Northwest National Laboratory, General Motors, Chrysler, Ford, U.S. Steel

Contractor: Pacific Northwest National Laboratory

Contract No.: DE-AC06-76RL01830

Objective

- Develop, validate, and disseminate a combined experimental and numerical method to describe statistically and quantify systematically the forming limits of welded aluminum alloys and high-strength steels.

Approach

- Develop a standard tool for weld process development that will systematically quantify failure probabilities during forming.
- Provide accurate, standardized methods of experimentally characterizing weld metal formability using unique but simple test methods available on the shop floor.
- Provide predictive models for more accurate forming simulations of tailor-welded blanks (TWBs) and hydroforming operations. Predict parts-per-thousand failure rates during production from finite element analysis.
- Characterize static/fatigue properties and forming behavior of several weld populations and correlate with statistical-based tool.

Accomplishments

- Established an industrially relevant procedure to determine the forming limit diagram (FLD) of welded DP600 steel alloys.
- Developed a more general procedure that can be applied to welded thin sheets.
- Completed the combined forming limit prediction for DP600, AA5182-6111 and AA5182 welded alloys.
- Quantified the combined FLD using the statistical approach for each welded alloy population.

- Conducted program review meeting in February 2008 to Industrial Team Advisory Committee.
- Participated in Plasticity 2008 and presented project-related work.

Future Direction

- With original equipment manufacturer (OEM) participation, validate the experimental and numerical methodology and general procedure generated with any existing TWB applications in a production environment.
- Complete all final work and submit journal articles detailing work and findings.
- Conduct final project presentation summarizing results with Industrial Team Advisory Committee.

Introduction

This work is a collaborative effort among DOE, Pacific Northwest National Laboratory (PNNL), the U.S. Automotive Materials Partnership (USAMP) team of the U.S. Council for Automotive Research, U.S. Steel, Olympic Controls, and Alcoa. This project will develop, validate, and disseminate combined experimental and numerical methods that systematically quantify the forming limits of weld materials in aluminum alloys and high-strength steels through a combination of experimental and deformation modeling analysis. This work will enable high-volume, robust deployment of TWBs and seam- and tailor-welded tubes in emerging materials. Figure 1 is a schematic of the project.

The deformation of weld materials and their limits of formability are important aspects to both TWB and hydroforming technologies. The conventional low-carbon steels used in automotive applications are easily fusion-welded using conventional technologies and suffer no appreciable strength degradation near the weld. Aluminum alloys are more difficult to weld than low-carbon steels due to high conductivity and reflectivity as well as low-molten viscosity. Aluminum also has a high propensity for porosity to form during fusion welding as well as hot cracking and heat-affected zone (HAZ) related issues in heat-treatable aluminum alloys. Many of the high-strength steel alloys that are finding increased application in the automotive industry suffer from degradation of strength in the HAZ.

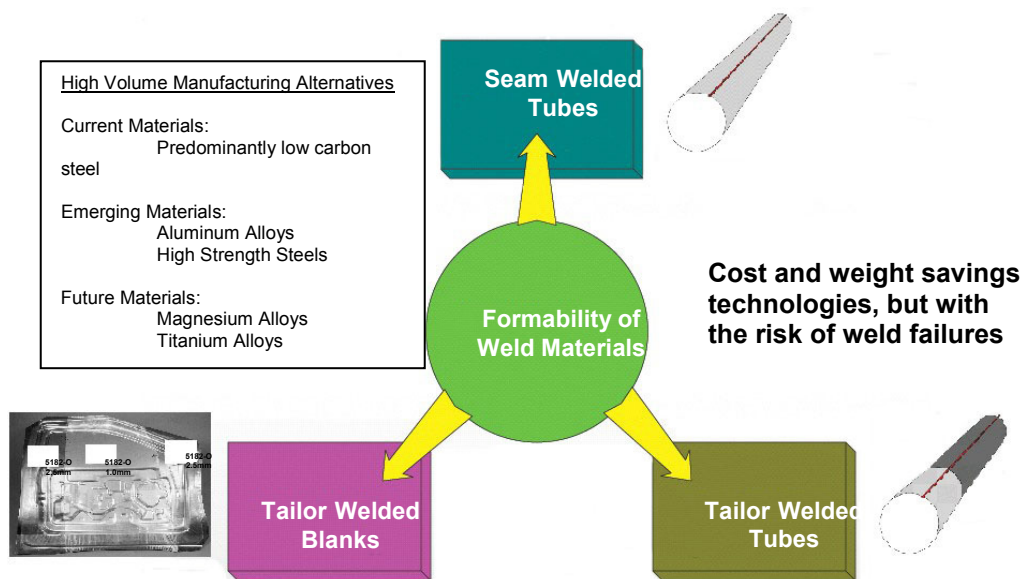


Figure 1. A schematic of the formability of weld materials project.

Further, nearly all fusion welds suffer from irregular geometries and elevated levels of surface roughness compared to the parent materials, which also influence formability and component performance.

This project focuses on developing a generalized numerical method to predict material-forming limits in weld materials and verifying deformation and forming limit predictions. The approach will rely on developing standardized test methods for weld material populations to establish a statistical description of material imperfection and mechanical properties in their weld region and developing statistically based forming limit diagrams (FLD) or continuum damage models that predict material failure in the weld region.

This project includes numerical model development, validation, and supporting experiments. A number of candidate weld methods were examined in combination with selected aluminum alloys and high-strength steels. The project materials will include 5000 and 6000 series aluminum and relevant high-strength steel alloys, including high-strength, low alloy; transformation-induced plasticity; and dual phase steels. The selection of sheet

materials and welding methods will be coordinated with the participating OEMs and will be representative of high-volume commercially viable materials and processing technologies.

The deliverables will include a standard procedure for weld material evaluation coupled with a numerical approach for establishing weld region forming limits. The results will also allow the evaluation and development of candidate weld processes and the interaction between materials and weld parameters. The overall objective is to develop test methods and experimental results to enable the widespread deployment of weight- optimized TWB and tube hydroforming and to avoid weld failures during production. Figure 2 is a schematic of the typical manufacturing process development.

During this fiscal year, much emphasis was spent on developing an industrially relevant procedure to determine the FLD of welded aluminum and high-strength steel alloys. A procedure was first applied to DP600 welded alloys and then generally modified, so the procedure may be applied to aluminum-welded alloys or any thin sheet-welded alloy to determine the forming limit. The following describes results to date and the development of the industrially relevant procedure.

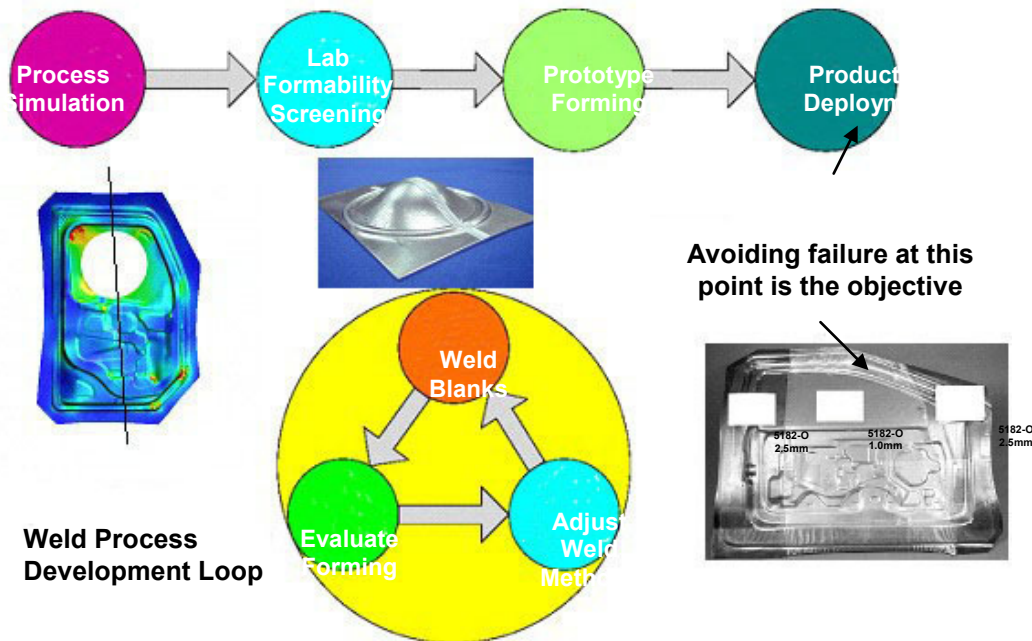


Figure 2. A schematic of the typical manufacturing process development.

M-K Method to Predict Formability

FLDs for the DP600 and 5182 welded to 6111 TWBs were generated using a Marciniak-Kuczynski (M-K) method approach that can track development of plastic strains in the monolithic sheet and weld materials under applied external loading. The model also tracks the evolution of imperfections and predicts the localization and failure of specimens. Theoretical FLDs are generated based on uniaxial tensile results and statistical probability. The level of imperfection that must exist in the specimens in order to describe the formability for each of the 30 longitudinal specimens is determined. A Weibull probability distribution is then applied to describe the longitudinal specimen imperfections, and the predicted FLD for the TWBs is generated.

Previously, the 5182-6111 full dome biaxial test experiments were compared to the theoretical FLD generated. Discrepancies of the model and biaxial experiments were observed, so all test results were combined in an FLD where the strain longitudinal to the weld and the strain transverse to the weld was plotted. The FLD of the parent sheet material (from literature) was also plotted. Results showed that there was a region in the FLD where the weld

will always fail and a region where the sheet will fail. In between is a “gray area” where either the weld or HAZ of the thin sheet 6111 material will dictate the failure.

Additional limited dome height tests were completed to investigate how the FLDs would be suppressed in these “gray areas.” Nine full dome width specimen tests and fifteen 4-in. width specimen tests were completed. Three different failure modes were observed among the full width specimens, and all 4-in. width specimens failed in the weld transverse to the weld. Modifications to the forming limit prediction were completed. The M-K model was extended to include weld thickness difference and two orientations of imperfection in the weld (schematic shown in Figure 3).

Work continued on the development of the FLD for the 5182-5182 TWB populations. Figure 4 shows the combined experimental results and compares these results to the monolithic 5182-O sheet FLD. These results indicate that our approach becomes more difficult to validate as the weld FLD becomes nearly identical to the thin sheet FLD.

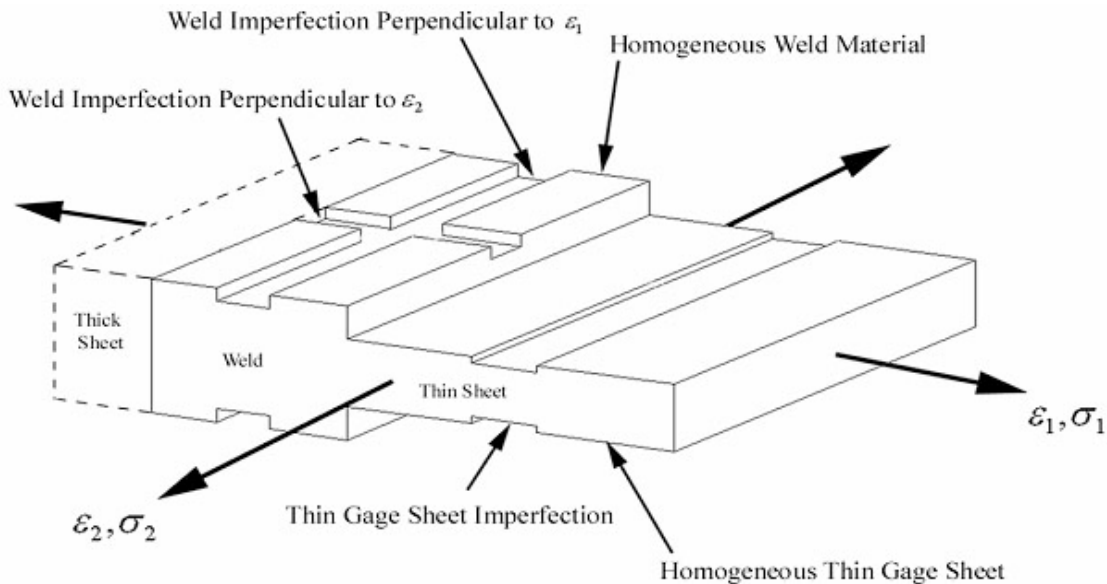


Figure 3. Schematic illustration of the M-K model extended to include weld thickness differences and two orientations of imperfection in the weld where ϵ_1 and ϵ_2 represent the major and minor strain, respectively, and σ_1 and σ_2 represent the associated stress for the major and minor strain, respectively.

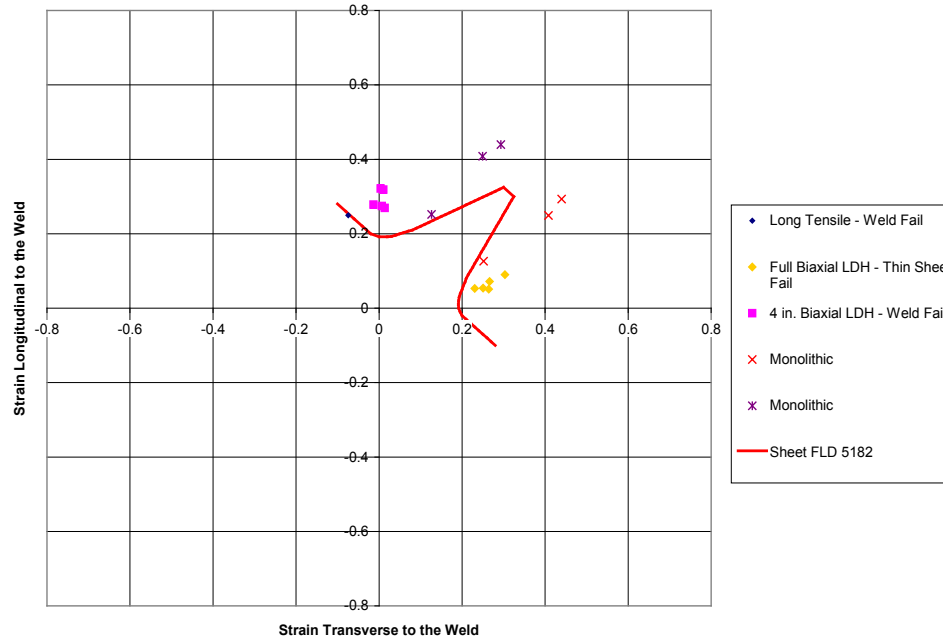


Figure 4. 5182-5182 friction stir welded materials combined test results and compared it to the FLD for 5182 monolithic sheet.

General Procedure in Determining the FLD of Welded Alloys

Currently, there is no industrial standard that describes the formability of TWBs that include the effects of the weld region. One of the goals of this project is to develop a procedure for industry to use by characterizing the variability of these materials and treating it probabilistically so we may have a better understanding of the operating envelope of these TWB materials. The general procedure was first applied to DP600 welded alloys. Figure 5 depicts the DP600 TWB FLD generated from the 10-step process described below. In-depth details of the industrially relevant procedure developed and the assumptions required will be published in future work.

1. Establish the thin (or the weaker) sheet FLD and draw a three-quadrant FLD where longitudinal strain is the ordinate (y-axis) and the transverse strain is the abscissa (x-axis).
2. Conduct approximately 30 longitudinal tensile tests and measure the “safe” level of strain in the thin sheet adjacent to the weld for each specimen.

3. Calculate the statistical distribution for the level of imperfection for the longitudinal specimens.
4. Conduct approximately 30 transverse tensile tests and measure the “safe” level of strain in the thin sheet adjacent to the weld for each specimen and *verify that no weld related failures occurred.*

Note: In previously reported work, experimental results showed that in the transverse weld condition, there was no fracture in the weld or in the heat affected zone of the DP600 welded specimens. Localization occurred in the thin sheet, and fracture was determined by the properties of the 1 mm parent sheet material.

5. Assume the acceptable failure rate for a given metal forming application (recommendation is 1 part per 1000).
6. Calculate the imperfection level for the longitudinal population that corresponds to the acceptable failure rate.
7. Calculate the “safe” level of strain along the longitudinal tensile direction that corresponds to the acceptable failure rate (Locate Point 1).

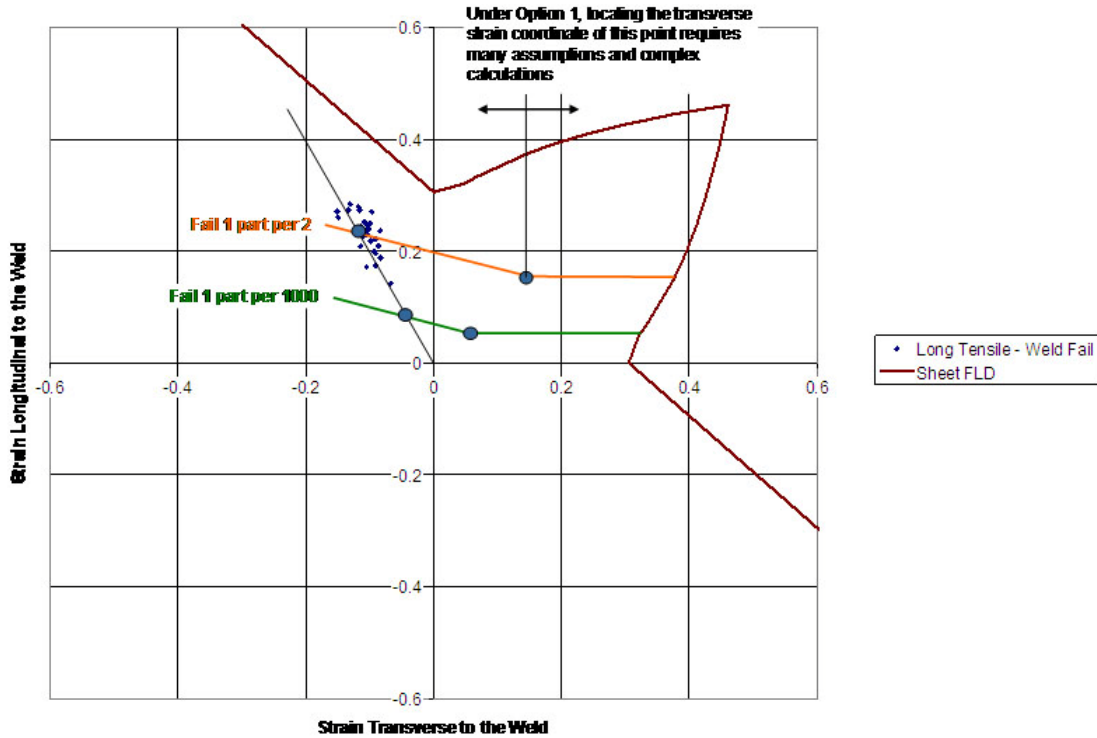


Figure 5. DP600 TWB FLD developed utilizing the industrially relevant procedure.

8. Calculate the strain path direction developing in the thin sheet when the weld is being loaded in plane strain longitudinal to the weld and place a point on the FLD that corresponds to the “safe” longitudinal plane strain and the transverse strain in the thin sheet (Locate Point 3).
9. Connect Points 1 and 3 via a line.
10. Draw a horizontal line from Point 3 horizontal to the transverse strain axis to the right of Point 3.

Further validation of the industrially relevant procedure is anticipated through plant trial validation. Five random blanks over several weeks will be gathered where the strain level achieved during forming would be determined. We will apply the PNNL procedure to predict the failure rate of a real production process.

We will track the failure rate in the plant and compare the predicted and actual failure rates.

Conclusions

From this investigation, the following conclusions were derived:

- Forming of welds has the potential to simultaneously reduce the cost AND weight of lightweight automotive structures.
- Emerging materials (aluminum and HSS) are generally more challenging to join and form.
- We developed methods/standards for describing the forming limits that include the effects of the weld region, which predicts forming failure rates at quantitative levels of deformation.

Further work will include preparing final validation and publications of the project work.

Presentations/Publications/Patents

1. "Forming Limits of Weld Material in Aluminum Alloys and High-Strength Steels." 2008. Presented to Industrial Team Advisory Committee, Southfield, MI. February 21.
2. "Formability and Strength of Dissimilar Aluminum Welds in Thin Sheets During Biaxial Stretching." 2008. Presented at Plasticity 2008, Kona, HI. January 7.
3. "Forming Limits of Weld Material in Aluminum Alloys and High-Strength Steels." 2007. Presented at U.S. Automotive Materials Partnership AMD Offsite Annual Review Meeting, Southfield, MI. October 25.

B. Impact Modeling and Characterization of Spot Welds

Principal Investigator: Zhili Feng

Oak Ridge National Laboratory

P.O. Box 2008, Oak Ridge, TN 37831-6095

(865) 576-3797; fax: (865) 574-4928; e-mail: fengz@ornl.gov

Co-Principal Investigator: Srdjan Simunovic

Oak Ridge National Laboratory

P.O. Box 2008, Oak Ridge, TN 37831-6164

(865) 241-3863; fax: (865) 574-7463; e-mail: simunovics@ornl.gov

Technology Area Development Manager: Joseph A. Carpenter

(202) 586-1022; fax: (202) 586-1600; e-mail: joseph.carpenter@ee.doe.gov

Field Technical Monitor: C. David Warren

(865) 574-9693; fax: (865) 574-6098; e-mail: warrencd@ornl.gov

Contractor: Oak Ridge National Laboratory

Contract No.: DE-AC05-00OR22725

Objective

- Develop a new, robust spot weld element (SWE) model that can accurately simulate the various deformation and fracture modes of advanced high-strength steel (AHSS) spot welds as a function of impact, welding conditions, and materials while maintaining computational efficiency and ease of use.
- Develop the implementation procedure to incorporate the SWE model in crash simulation finite-element analysis (FEA) codes used by automotive crash modelers.
- Generate a companion experimental database on the performance of AHSS spot welds under various loading conditions and deformation rates to support and validate the modeling approach.

Approach

- Develop a new SWE model and associated constitutive models.
- Perform modeling and characterization of weld microstructure and related properties.
- Integrate the SWE model and weld process and microstructure model.
- Perform weld deformation and failure behavior testing under different dynamic-loading conditions.

Accomplishments

- Developed the initial version of the SWE model.
 - Capable of handling weld geometry and weld property gradient.
 - Capable of predicting different fracture modes and fracture load limits experimentally observed in impact tests.
- Developed the initial version of an integrated electrical-thermal-mechanical-metallurgical resistance spot weld model.
 - Capable of predicting weld geometry, microstructure, and microhardness distributions.
 - Includes user-friendly input interface for welding parameters, sheet thickness, and steel chemistry.

- Collected baseline spot weld impact test data on dual phase (DP) 780 and draw-quality, semi-killed (DQSK) steels.
 - Characterized effects of impact speeds and loading modes.
 - Created web-based database for user-friendly interactive data analysis and retrieval.

Future Direction

- Further expand and validate the SWE model to cover a wide range of AHSS grades and spot weld configurations to demonstrate the applicability of the SWE model for the current generation of AHSSs.
- Extend the SWE model to the weld bond for AHSSs.
- Extend the SWE model to other materials and joining processes.
 - Joining of steels to other materials [such as aluminum (Al) alloys, magnesium alloys, polymer composites] for multi-material body structure.
 - Friction-bit joining, friction-stir joining, laser welding.
- Continue failure criteria evaluation and development.
 - Incorporate the effect of heat-affected zone (HAZ) softening in ultra-high-strength steels and Al alloys.
 - Develop failure criteria for other processes, including adhesive bonding.
- Further refine SWE formulation for robustness.

Introduction

A primary factor that drives increased use of AHSSs in auto-body structures is their ability to drastically improve crash performance while reducing the weight. Resistance spot welding (RSW) is by far the most common joining process used in automotive manufacturing. Typically, there are thousands of spot welds in a vehicle. Because the separation of spot welds can affect the crash response of a welded structural component, the static and dynamic behavior of spot welds has been one of the critically important considerations in vehicle design and manufacturing.

RSW of AHSSs presents unique technical challenges for automotive structural applications. Due to their high carbon and alloying element contents, AHSSs are considerably more sensitive to the thermal cycle of welding than the conventional steels used in auto-body structures. The higher grade AHSSs (e.g., DP 800/1000, TRIP steels, and boron steels) are more difficult to weld and more susceptible to forming brittle microstructures and solidification-induced defects in the weld region. In addition, HAZ softening can occur. Therefore, resistance spot welds of AHSSs can exhibit very different structural performance characteristics than welds of conventional steels. For example, AHSS spot welds can fail under different failure modes (button pullout, interfacial,

or mixed). In addition, impact experiments on joints and structural components (top-hat and double-hat sections) have shown that resistance spot welds have different responses under static and dynamic loads. The spot-welded structural performance among different AHSSs can be drastically different and highly dependent on the grades and types of AHSS. Furthermore, there can be considerable variations in microstructure and properties in the weld region for a given type and grade of AHSS made by different steel suppliers due to differences in steel chemistry and the processing routes used.

In recent years, computer-aided engineering-(CAE-) based simulation of dynamic (impact) behavior of auto-body structures during crash tests has become an indispensable tool that enables rapid and cost-effective design and engineering of crash-resistant auto-body structures. This program aims to develop a new spot weld model, supported by experimental data, which can be implemented in crash-simulation FEA codes used by automotive crash modelers. The essential feature of this new model will be its ability to handle various deformation and fracture modes, the effects of microstructural and strength changes in AHSS spot welds, and the deformation rates and loading modes encountered in vehicle crash. A three-pronged approach has been adopted in the development of the new spot weld model:

- development of a robust new SWE model with the complexity to incorporate weld geometry and microstructure effects and the associated constitutive models for use in CAE simulation;
- development of an integrated electrical-thermal-mechanical-metallurgical spot weld process model to generate the weld geometry, microstructure, and residual-stress results needed by the SWE model; and
- development of a companion weld characterization and impact test database for development and validation of the new spot weld model.

In recognition of the complexity and scope of efforts required to develop and mature this new model for the wide variety of AHSSs currently used in auto-body structures, this project has been divided into two phases. Phase I is an 18-month concept-feasibility effort aimed at developing the initial version of the SWE model and generating the companion testing data for an initial set of steels, weld configurations, and impact testing conditions. Phase II will be a comprehensive technical-feasibility research and development process that will cover a wider range of materials, thickness ranges, and weld configurations and microstructures to refine, improve, mature, validate, and demonstrate the SWE model for eventual implementation in CAE by industry users.

The progress made in Phase I of the project is summarized in the fiscal year (FY) 2007 progress report and this report. Phase I is jointly sponsored by the DOE Lightweighting Materials area and the Auto/Steel Partnership (A/SP) Strain Rate Characterization Program (see report 5.F).

Materials, Welding, and Testing

Details on steel selection, welding, weld microstructure characterization, and impact testing of the spot welds are given in the FY 2007 progress report.

Two steels, dual-phase AHSS DP 780 steel (1.15 mm thick) and DQSK mild steel (1.0 mm thick), were selected for the initial development in Phase I. For each steel, the welding schedule was

varied to produce three different weld nugget sizes acceptable to the industry specification for studying the effects of weld size on the fracture behavior of spot welds in impact testing.

Microstructural analyses were performed to characterize the microstructure and microhardness gradients and the weld defects (if any) in the weld and HAZ of the spot welds. The microstructure and microhardness results were used to validate the weld process model for RSW.

Both dynamic and static tests of the spot welds, in lap-shear, cross-tension, and mixed torsion/tension loading configurations, were performed at four loading velocities: quasi-static, 2.6 m/s (5.8 mph); 3.6 m/s (8.1 mph); and 5.8 m/s (12.5 mph). A drop-tower impact test machine was used for the impact tests.

The fracture modes and peak loads to failure of all spot welds were recorded during the test. The impact testing results are retrievable online by A/SP members. Dependency of fracture mode and peak load on weld size, loading mode, and loading rate were observed. These data were used to validate the SWE modeling approach.

Weld Microstructure and Property Modeling and Characterization

An integrated electrical-thermal-mechanical-metallurgical welding process model for electric RSW is used in this project. It is based on earlier work [1] with further refinement of the microstructural model for AHSS.

The RSW process model predicts the weld size, microstructure, and residual stresses in a spot weld based on the following user inputs.

- Steel chemistries and base metal microstructure.
- Surface coating.
- Sheet stackups.
- Welding conditions (current and electrode force).
- Electrode geometry.

A key feature of this integrated weld process model is that it predicts the microstructure

evolution based on calculations of the thermodynamics and kinetics of steel phase-transformation processes. There is no need to experimentally measure the continuous cooling transformation curves for a given steel, an impossible task for all possible thermal cycles experienced in different locations of the weld and HAZ of a spot weld.

The integrated weld process model was applied to the two steels and different welding conditions used in Phase I. The simulation results compared well with measurement results of the weld microstructure and microhardness distributions in the spot welds. Figures 1 through 4 show examples of the weld process modeling results and compares the results with the experimental hardness measurement results.

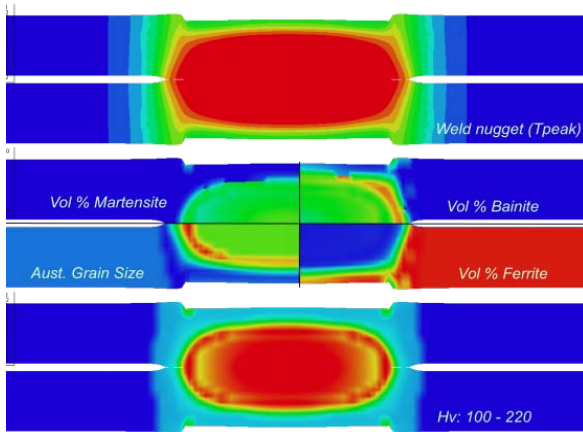


Figure 1. Predicted weld nugget as represented by: the peak temperature (top), volume fractions of different phases (middle), and microhardness distribution (bottom) in a DQSK spot weld.

The predicted microhardness results were then converted to the yield strength [1] and used in the SWE formulation.

Development of Spot Weld Element

Spot welds in finite-element method impact simulations are usually modeled with two submodels: (1) a kinematics model of the joint and (2) the associated constitutive model describing the material-related response of the joint. Currently, the kinematics of the joint is primarily modeled as point-to-point connection by means of

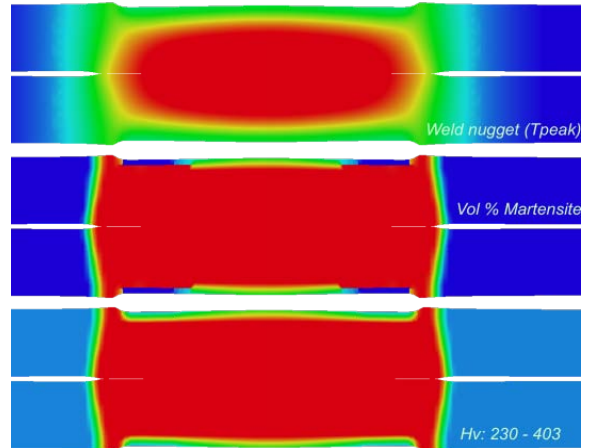


Figure 2. Predicted weld nugget profile as represented by: the peak temperature distribution (top), volume fractions of different phases (middle), and microhardness distribution (bottom) in a DP 780 spot weld.

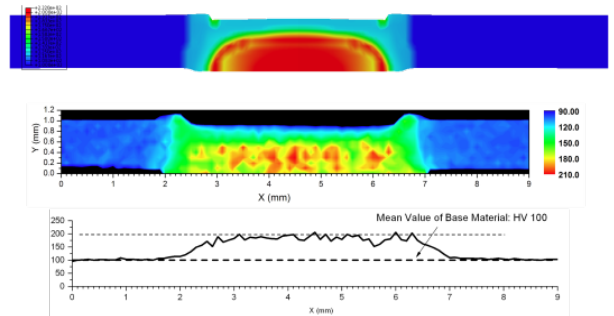


Figure 3. Comparison of microhardness distribution in a DQSK spot weld: (top) prediction, (middle) microhardness measurement, and (bottom) line plot along the middle plane of the steel sheet.

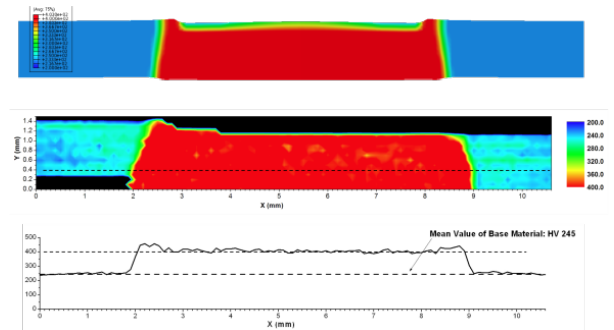


Figure 4. Comparison of microhardness distribution in a DP 780 spot weld: (top) prediction, (middle) microhardness measurement, and (bottom) line plot along the middle plane of the steel sheet.

flexible or rigid (i.e., constrained) line finite elements.

The line connection is restricting the constitutive spot weld models to force-based laws. This in turn requires new experiments for model parameters with new RSW configurations. One of the principal problems with beam-based kinematics models in AHSS spot welds is that the stress and strain distributions in the weld area are not accurately represented. For RSW in conventional steel structures, the dominant failure mode is the button pullout, and the inadequate calculation of the shear stress may not be a major concern in impact simulation of vehicles. However, for AHSS RSW, accurate determination of the shear stress may be critical because of the reported interfacial failure or mixed interfacial plus pullout failure mode. In addition, the multiple failure modes and the changes in failure modes under different loading conditions require development of more versatile failure criteria based on the fracture and damage mechanics principles than the resultant force-based ones. From the structural stiffness perspective, the bar and beam models typically yield acceptable accuracy under tension, out-of-plane torsion, and bending loads. For in-plane torsion and shear, the stiffness values are highly inaccurate. The brittle fracture associated with the interfacial failure of the spot weld is more likely during impact, where plastic deformation of the base material may be constrained by large elastic stress fields. Compared to a gradual increase in hardness in the HAZ in mild steel resistance spot welds, the AHSSs exhibit a sharp hardness change that adds to brittleness and notch sensitivity of the joint.

The objective of this research was to develop an RSW model that would be able to predict the stress distribution in the weld zone and would be computationally feasible for crash simulations. The recent RSW models based on solid elements inserted between shell elements of the sheet material have shown much better accuracy than the line-based elements. We have extended that approach to the model configurations illustrated in Figure 5. The schemes depict through-thickness direction of the spot weld.

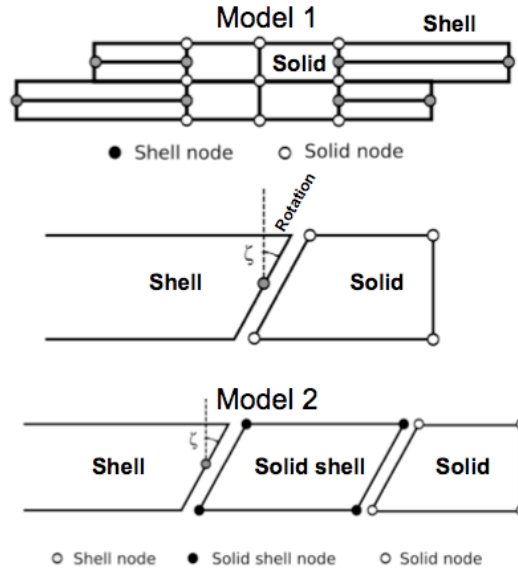


Figure 5. Configuration of the spot weld model in the through-thickness direction. Model 1 has shell elements in the HAZ and the plate; whereas Model 2 used an eight-node solid shell for the HAZ. The middle figure shows the coupling between the four-node shell and solid.

The models have compatible connections between the plate (shell) and the nugget (solid) regions. The principal difficulty is the element meshing of the region, but with the current computational design tools such connections should be easily managed.

Additional simplification of the connection comes from the fact that the inner region of the spot weld is relatively stress-free compared to its periphery. Accordingly, the inner region of the weld can be replaced by computationally inexpensive rigid elements or, equivalently, kinematic constraints. The constraints computationally stabilize the solid elements in the deformable region of the spot weld and provide additional mass that can be used for computational speedup of the region using mass time-scaling.

Possible failure regions in the new spot weld connection are shown in Figure 6. The stress-strain values in those regions can be used to evaluate various fracture criteria that would initiate failure of the spot weld. In the current research, a simple failure criterion based on equivalent strain to failure was used. The material properties in the weld region were based on the

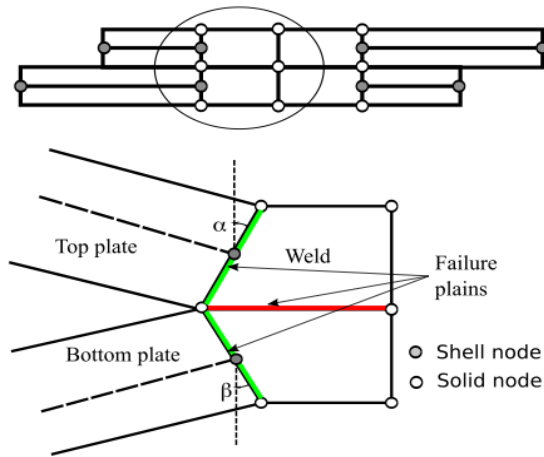


Figure 6. Failure zones in the spot weld model.

hardness measurements and simulations. Base material properties were scaled with the simulated/measured hardness coefficient, and equivalent strain-to-failure was reduced accordingly. This constitutes a very simplistic model that will need to be replaced by more accurate criteria in the future.

Figure 7 shows the simulation of the lap-shear test with small spot weld diameter. The failure of the spot weld in simulation and experiments was along the interface between the two connected sheets.

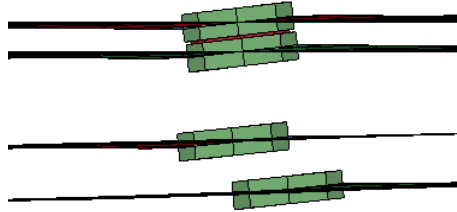


Figure 7. Lap-shear test simulation for small spot weld diameter.

The resulting force comparison is very close given the experimental scatter and the simplicity of the failure model (Figure 8). Figure 9 shows the simulation of the lap-shear test for large spot weld diameter. The resulting force comparison is again reasonably close to the resulting force and stiffness of the assembly (Figure 10).

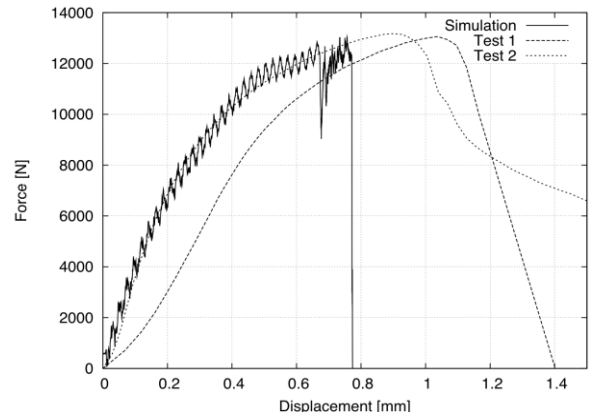


Figure 8. Comparison of the resulting force for experiments and simulations for small spot weld diameter.

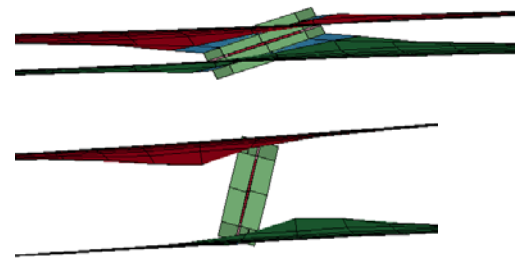


Figure 9. Lap-shear test simulation for large spot weld diameter.

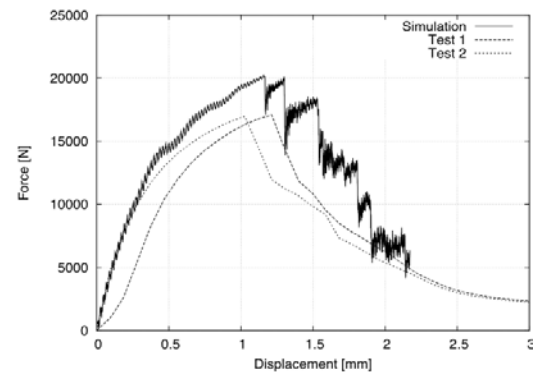


Figure 10. Comparison of the resulting force for experiments and simulations for large spot weld diameter.

The model accurately recovers geometry effect without the need for separate experiments for the new spot weld configuration. This is because the failure condition, even though very simple, is based on material properties instead of the extrinsic properties of the overall joint. The model was also compared with other spot weld configuration experiments conducted during the

project and has shown good agreement for the relatively simple failure criteria used. New experiments are planned for creating the complex states of stress in spot welds that can be used for further model refinement and development of the failure criteria for the spot welds.

Reference

1. Z. Feng et al., "Modeling of Resistance Spot Welds—Process and Performance," *Welding in the World*, **45**(11/12), pp. 18–25 (2001).

C. Friction Stir Spot Welding of Advanced High-Strength Steel

Principal Investigator: Michael L. Santella

Oak Ridge National Laboratory

P.O. Box 2008, Oak Ridge, TN 37831-6096

(865) 574-4805; fax: 865-574-4928; e-mail: santellaml@ornl.gov

Principal Investigator: Glenn J. Grant

Pacific Northwest National Laboratory

902 Battelle Boulevard, P.O. Box 999, Richland, WA 99352

(509) 375-6890; fax: (509) 376-6034; e-mail: Glenn.Grant@pnl.gov

Principal Investigator: Yuri Hovanski

Pacific Northwest National Laboratory

902 Battelle Boulevard, P.O. Box 999, Richland, WA 99352

(509) 375-3940; fax: (509) 376-6034; e-mail: Yuri.Hovanski@pnl.gov

Technology Area Development Manager: Joseph A. Carpenter

(202) 586-1022; fax: (202) 586-1600; e-mail: joseph.carpenter@ee.doe.gov

Field Technical Co-Monitor: C. David Warren

(865) 574-9693; fax: (865) 574-6098; e-mail: warrencd@ornl.gov

Field Technical Co-Monitor: Mark Smith

(509) 375-4478; fax: (509) 375-4448; e-mail: mark.smith@pnl.gov

Contractors: Oak Ridge National Laboratory (ORNL) and Pacific Northwest National Laboratory (PNNL)

Contract No.: DE-AC05-00OR22725 & DE-AC06-76RLO1830

Objective

- Develop friction stir spot welding (FSSW) as a superior method to join advanced high-strength steels (AHSSs).
- Phase 1 activities addressed the critical questions of whether there are tool materials available that have potential for reasonable life and whether friction stir spot welds (FSSWs) made in AHSSs are feasible and can demonstrate similar or better mechanical performance than welds made by conventional processes like resistance spot welding (RSW).
- Phase 2 activities seek to increase joint strength through a more systematic investigation into weld process parameters and tool design. This will be accomplished primarily by using new tools and refined operating parameters, the selection of which will be guided by analysis of process output data, microstructure analysis, and strength testing.

Approach

- The project is a collaboration between ORNL and PNNL, and includes an advisory committee with representatives from Chrysler, Ford, General Motors (GM), two automotive steel suppliers, and a friction stir welding tool supplier.
- Produce lap-shear specimens and perform lap-shear tests to correlate tensile shear strength with processing parameters and microstructures.

Accomplishments

- Made hundreds (~500) of FSSWs on uncoated dual phase (DP) 780, galvanized DP 780 (DP 780GA), and uncoated hot-stamp boron steel (HSBS) using a wide range of welding conditions.
- Compiled data on the effects of weld time, tool rotation speed [revolutions per minute (rpm)], and tool shape on appearance, bonding, fracture, microstructures, properties, and process loads.
- Performed mechanical tests on Phase 1 DP 780 and HSBS lap-shear coupons. While overall strengths for certain weld parameters were in the range of acceptable values defined by the American Welding Society (AWS) specification for RSW of steel, the specific strength under nearly every condition exceeded the minimum stress condition.
- Performed mechanical testing of FSSWs joined using Phase 2 tools, which showed dramatic increases in lap-shear strength when compared to the results from welds produced with Phase 1 tools.
- Determined that for weld times of 4 seconds (s), the maximum lap-shear tensile strengths measured are 17 kN for DP 780, 22 kN for galvanized DP 780, and 16 kN for HSBS. All of these values exceeded the minimum specified in the AWS specification for RSW.
- Determined that lap-shear strengths tend to increase with removal of mill, which indicated that surface condition of the sheets has an important influence on mechanical properties and bonding.
- Determined that for otherwise identical welding conditions, increasing tool rotation speed from 800 to 1,600 rpm increased strength values for spot welds made with DP 780 and DP 780GA. Using a two-step schedule rather than a one-step schedule had a similar effect. Metallographic examinations indicated this is at least partly related to increased size of bonded area.
- Made and evaluated stir tools of six different tool materials. These materials are tungsten 25% rhenium alloy, polycrystalline cubic boron nitride (PCBN), silicon nitride (Si_3N_4), titanium diboride (TiB_2), tungsten carbide-cobalt, and a cermet made of complex carbides bonded by a refractory metal alloy.
- Determined PCBN has the most promise as a stir tool material. Wear rates in PCBN tools are very low, although the overall durability, availability, and cost may prove prohibitive for widespread commercial applicability.
- Confirmed that tool shape can have a significant influence on lap-shear strength.

Future Direction

- Evaluate performance of friction spot welds in the cross-tension test.
- Evaluate the response of DP 780 with a broader range of zinc coatings (hot-dipped and electrogalvanized, in particular), similar to what will be encountered in the manufacturing environment. Modified Al-Si coatings will also be evaluated for HSBS.
- Continue to evaluate tool materials, including reformulated PCBN and Si_3N_4 .
- Continue detailed microstructure characterization including fracture behavior.
- Continue study of the relation of strength to sheet surface condition.
- Initiate fatigue testing of joints.
- Develop nondestructive evaluation (NDE) strategies.

Introduction

The technology for implementing FSSW of aluminum in automotive manufacturing environments exists. C-gun-type FSSW heads have been developed and adapted to robotic

systems that are now commercially available for FSSW of aluminum alloys. This project addresses the questions of whether the FSSW process is viable for joining AHSSs and whether FSSW has advantages over conventional processes like RSW.

Preliminary work on FSSW of AHSSs suggested that several features of the process (fine-grained microstructure in the nuggets of AHSSs, potentially higher-strength joints and higher energy absorption in crash, low energy consumption and environmental emission during manufacturing) may give FSSW cost and energy saving advantages over RSW. In addition, the process may be viable for high-strength, lightweighting alloys that are difficult to join using conventional techniques (DP 1000, martensitic steels such as HSBSs, etc.).

Important questions remain about effective, economical application of FSSW to AHSSs. Critical questions being addressed in this study include the following.

- Are tool materials available that have potential for reasonable life?
- Are joint strengths of FSSWs comparable to or better than those of welds produced with conventional processes?
- Are manufacturing conditions appropriate (cycle time, tool wear, process robustness and sensitivity to production variation)?
- Do FSSW-produced joints have any advantage for NDE or for real-time process control over RSW?
- Are total life-cycle costs appropriate?
- Can the process be modeled and predictive tools be developed to aid designers?

If the effectiveness of FSSW for joining AHSSs is established, this could accelerate the insertion of these high-strength lightweighting alloys into automotive body construction to help meet FreedomCAR goals.

Approach

The primary goal of this project is to characterize the responses of AHSSs to FSSW to establish whether FSSW is an acceptable method for joining AHSSs and can be incorporated in current manufacturing processes. The project is organized into two phases. Phase 1 activities addressed the critical questions of whether there are tool materials available that have potential for reasonable life and whether FSSWs made in AHSSs could develop strengths comparable to

those in welds made by conventional processes like RSW. Phase 2 focuses on the factors crucial to industrial implementation of FSSW; therefore, the second phase of the project concentrates on evaluation of several specific targets including cycle time, tool durability, process robustness, and repeatability.

The Phase 1 results and the initial work under Phase 2 highlight two important challenges: the development of robust tool materials and the development of the weld parameters needed to achieve consistently high joint strengths. Both sets of issues, those related to tooling and those related to joint strength, appear to be interrelated.

Currently, PCBN is the most durable, effective material from which to make stir tools for welding AHSSs; however, PCBN is relatively expensive, difficult to machine into the needed shapes, and not widely available for purchase. These characteristics significantly complicate modifying tool designs, but such modification is a critical element in maximizing joint strengths. In addition, the intrinsic durability of PCBN has not been well characterized. Thus, there is considerable interest in identifying and evaluating alternatives to PCBN, particularly any that would reduce tool costs and improve durability.

A second set of challenges identified in prior work relates to developing consistently high joint strengths. Joint strengths are being obtained that compare favorably with minimum values specified in industry standards for spot welds such as AWS D8.1M [1]. However, the consistency of obtaining these strength levels must be improved. In addition, welding times must be minimized. These conditions can be met by increasing the bonded area of FSSWs.

In addition to addressing the issues discussed above, in Phase 2 we intend to evaluate joint microstructures and mechanical properties, assess the potential for in-process NDE, and establish the framework of a design database for spot friction-welded structures. The project is a 50-50 collaboration between ORNL and PNNL, and it includes an advisory committee with representatives from Chrysler, Ford, GM,

ArcelorMittal Steel Corp., and Gestamp U.S. HardTech, Inc.

Materials and Experimental Details

Until recently, most of this work was done using two uncoated AHSSs: DP 780 and an HSBS sourced from a Swedish supplier, the parent of U.S. HardTech. The DP 780 is 1.5 mm thick sheet; the thickness of the HSBS is 1.4 mm. More recently, a lot of galvanized DP 780 (U.S. Steel) was included in the activities. The nominal thickness of this sheet was also 1.5 mm. [The suffix GA is added to specifically identify galvanized steel (e.g., DP 780GA) and results obtained with it.]

The FSSW performed during Phase 1 as well as during the initial portion of Phase 2 was done almost exclusively with PCBN tools. However, several lower-cost alternatives are being evaluated for FSSW tool materials during the Phase 2 program, including Si₃N₄, TiB₂, and a new tungsten-based cermet alloy.

All spot welds are made in displacement-control mode by varying the parameters of tool plunge depth and tool plunging rate. In addition to these control parameters, a number of other process variables are typically recorded for each weld, including weld time, spindle torque, normal force, and temperature on the back side of the two-sheet “stackups.” This additional information is archived for future use and analysis. Joint strength is evaluated by tension testing lap joints to determine their shear-tension strengths. Strengths are correlated with processing parameters and microstructures. Microhardness

mapping is also being used to assess the characteristics and properties of the joints.

Results and Discussion

Results from the lap-shear testing are presented in Tables 1–4. Tabulated data include the tool rotation speed, the number of programmed steps, the maximum measured load on the tool during welding, the maximum measured temperature, the actual values from lap-shear testing, and the average lap-shear strength value. The maximum tool load was determined by a load cell integrated into the spindle of the MTS ISTIR machine. Temperatures were measured with a thermocouple embedded in the supporting anvil that contacted the bottom of the two-sheet stackups. The thermocouple was located on about the centerline of the stir tools.

Several trends are apparent in the data. For the uncoated DP 780, there was a clear tendency for both lap-shear strength and maximum temperature to increase when using a two-step rather than a one-step weld procedure. This occurred at both 800 and 1,600 rpm. Also, increasing tool rotation speed with a given weld procedure tended to increase both lap-shear strength and maximum temperature. These trends were consistent for both stir tool shapes. The zinc coating did not have a detrimental effect on lap-shear strength, and in three of the four combinations, spot welds made with the DP 780GA had higher strengths than their uncoated counterparts. For identical welds, measured temperatures were lower for DP 780GA. This could be due either to the ceramic coating used on the backing anvil for the welds or to the effect of zinc reducing the initial friction coefficient between stir tools and sheet.

Table 1. Lap-shear test results for DP 780 steel welded with BN77 tool.

Rpm	No. of steps	Max. tool load (kN)	Max. temp. (°C)	Actual lap-shear strength values (kN)	Avg. lap-shear strength (kN)
800	1	32.5	410	4.8, 4.4, 4.0	4.4
800	2	33.0	537	7.5, 8.3, 8.4	8.0
800GA	2	40.8	493	10.8, 10.8, 11.8, 11.6	11.3
1,600	1	23.7	510	9.5, 9.7, 9.7, 9.4	9.6
1,600	2	31.3	641	10.4, 12.4, 11.5, 10.6	11.2
1,600GA	2	32.7	591	11.2, 11.5, 11.5, 10.7	11.2

Table 2. Lap-shear test results for DP 780 steel welded with BN46 tool.

Rpm	No. of steps	Max. tool load (kN)	Max. temp. (°C)	Actual lap-shear strength values (kN)	Avg. lap-shear strength (kN)
800	1	29.8	452	7.9, 8.2, 9.1	8.4
800	2	38.2	645	13.6, 14.7, 15.7	14.7
800GA	2	49.1	534	14.7, 16.4, 15.9, 14.1	15.3
1,600	1	34.3	606	10.3, 9.8, 11.0	10.4
1,600	2	31.8	712	17.4, 13.4, 16.0	15.6
1,600GA	2	32.1	683	22.6, 18.1, 17.0, 14.3	18.0

Table 3. Lap-shear test results for HSBS welded with BN77 tool.

Rpm	No. of steps	Max. tool load (kN)	Max. temp. (°C)	Actual lap-shear strength values (kN)	Avg. lap-shear strength (kN)
800	1	31.7	408	10.1, 10.0, 10.6	10.2
800	2	41.1	539	10.7, 12.1, 11.6	11.4
1,600	1	24.5	545	10.8, 11.0, 11.6	11.1
1,600	2	32.7	646	11.4, 11.4, 10.0	10.9

Table 4. Lap-shear test results for HSBS welded with BN46 tool.

Rpm	No. of steps	Max. tool load (kN)	Max. temp. (°C)	Actual lap-shear strength values (kN)	Avg. lap-shear strength (kN)
800	1	32.8	471	10.0, 8.0	9.0
800	2	44.2	633	12.0, 12.6	12.3
1,600	1	35.1	593	8.9, 10.5	9.7
1,600	2	30.8	717	15.0, 16.1	15.5

An initial reduction in friction properties may be more likely since maximum loads also tended to be higher for the DP 780GA. In all cases except spot welds of HSBS with the BN77 stir tool, maximum loads were experienced early in the plunges regardless of tool design.

The effect of rotation speed on temperature is expected because heat is generated in friction stir welding by two mechanisms. One is through friction at the interfaces of the tool surfaces and the workpiece material; the second is through viscous dissipation of metal flow in the vicinity of the tool [2–5]. A simplified view [6] indicates that temperature rise, ΔT , at a fixed location and set of conditions during friction stir welding can be expressed as

$$\Delta T \propto \frac{\mu P \omega}{K},$$

where μ is a friction coefficient, P is a pressure related to tool force, ω is tool rotation speed, and K is a constant. Increasing tool rotation speed has a direct effect on increasing temperature in the stir weld zone.

Using a two-step welding procedure at fixed rotation speed produced higher lap-shear strengths than a one-step schedule basically because a larger stir tool-sheet surface area was engaged for a longer period of time. This was determined by first associating the projected area of the BN77 and the BN46 tools with distance from their tips. A coordinate measurement machine was used to

determine the variations of tool radius with axial distance for both stir tools. These values were then used to calculate the variations of total projected area with axial distance, as shown in Figure 1. The relationship between axial distance from the tool tip and total projected area was then used to convert the tool load-time responses during welding into pressure-time data. An example of the differences between the one-step and the two-step welding procedures is shown in Figure 2

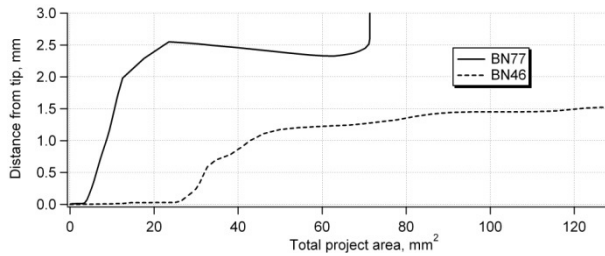


Figure 1. Variation of total projected area with axial distance from stir tool tips.

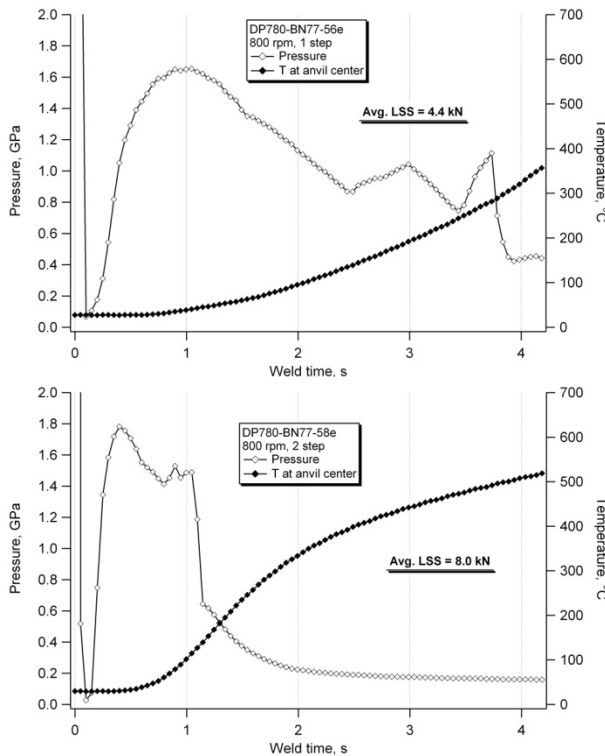


Figure 2. Variations of pressure and temperature for spot welds of uncoated DP 780 made at 800 rpm with either a one-step (top) or a two-step (bottom) welding procedure.

for spot welds made at 800 rpm with the BN77 tool on uncoated DP 780. Both the pressure and temperature are plotted with weld time in Figure 2.

The one-step approach involves a peak pressure early in the process near 1 s weld time, but the temperature at the pressure peak is relatively low. In addition, projected area at the pressure peak is also relatively small. The BN77 stir tool did not fully engage the sheet metal until this weld was about 80% complete. In the two-step approach, the stir tool became fully engaged with the sheet metal in about 1 s. From that point until the 4 s weld time was reached, the spinning tool continued to heat the weld zone and to maintain it under a relatively steady pressure. FSSWs appear to be characterized by regions of intense stirring near the stir tool-sheet metal interfaces, and this observation is consistent with metal flow analysis in the process [7]. However, interface bonding extends beyond distances where intense stirring occurs. This implies that diffusional processes (i.e., diffusion bonding) help to create the bonded interfaces of FSSWs.

Both pressure and temperature are important to diffusion bonding processes [8]. Thus, the higher strength of the two-step welds must be the result of having high projected area engaged with the sheet for relatively longer times at higher temperatures.

The overall characteristics of the pressure-time and temperature-time signatures of welds made with the BN46 stir tool were similar to those made with the BN77 tool. However, the peak pressures reached with the BN46 tool were lower by about 40%. Likewise, the temperature profiles were similar in shape, but those for the BN46 tool were higher by 50–100°C throughout the welding. This would be caused by the greater area of engagement of the BN46 tool with the sheet at any point during the welding. The characteristics of the pressure-time and temperature-time signatures were not substantially influenced by the presence of zinc on the DP 780GA. Analysis of the machine output data from welds of the HSBS are incomplete at the present time.

Unlike the behavior of DP 780 and of the HSBS welded with the BN46 stir tool, the lap-shear strengths of all welds made in HSBS with the BN77 stir tool (Table 3) were relatively insensitive to changing weld conditions. At the moment, it can only be suggested that this is related to the pin length on the BN77 tool. In friction spot welding of aluminum alloys, for example, it has been found that, for a set pin length, spot-welding condition, and metal thickness, lap-shear strength will increase with plunge depth up to a certain point. As plunge depth increases further, lap-shear strength values will reach a plateau and eventually start decreasing due to excessive thinning of the top sheet. It is clear that the BN77 pin length and HSBS thickness put this combination in a region of welding parameter space near a lap-shear strength plateau. This behavior appears analogous to that of aluminum alloys.

The ranges of lap-shear values presented in Tables 1–4 can be placed in perspective by comparing them to values required for resistance spot welds on the same steels. AWS D8.1M [1] was used to calculate minimum required shear strengths for both steels. The minimum values were calculated using tensile strengths of 790 MPa for DP 780 and 1,500 MPa for the HSBS. The results for required lap-shear strengths are 10.3 kN for DP 780 and 12.0 kN for the HSBS. The tabulated data show that the minimum values can be met for FSSW of either uncoated or galvanized DP 780 using a two-step schedule and either the BN77- or the BN46-type stir tool. The minimum value can also be met for the HSBS using the two-step process and the BN46 stir tool.

Conclusions

Lap-shear testing showed that for otherwise identical welding conditions, increasing tool rotation speed from 800 to 1,600 rpm increased strength values for spot welds made with DP 780 and DP 780GA. Using a two-step schedule rather than a one-step schedule had a similar effect. Spot welds made with either tool and a two-step schedule had lap-shear strengths that exceeded the required minimum value of 10.3 kN for resistance spot welds.

Lap-shear testing showed that spot welds made in the HSBS with the BN77 stir tool were relatively insensitive to tool rotation speed and weld schedule strategy. It was suggested this was related to the ratio of pin length to sheet thickness, but no conclusive evidence was provided to support the claim. The lap-shear strengths of this group of spot welds were all in the range of 10–11 kN, slightly below the minimum value of 12 kN required of resistance spot welds

Similar to DP 780, increasing tool rotation speeds from 800 to 1,600 rpm or using a two-step rather than a one-step weld schedule increased the lap-shear strength of spot welds made with the BN46 stir tool on the HSBS. The minimum shear strength required for resistance spot welds of 12 kN was exceeded for the HSBS using the two-step process and the BN46 stir tool.

Presentations/Publications/Patents

1. Y. Hovanski, M. L. Santella, and G. J. Grant, "Friction Stir Spot Welding of Hot-Stamped Boron Steel," *Scripta Materialia*, **57**, pp. 873–876 (2007).
2. Y. Hovanski, M. L. Santella, and G. J. Grant, *Friction stir spot welding of advanced high strength steels*, presentation at MS&T, September 2007.
3. G. J. Grant, Y. Hovanski, and M. L. Santella, "Friction Stir Spot Welding of Advanced High Strength Steels for Automotive Applications," in A. M. da Silva, J. F. dos Santos, and G. Amancio (eds.) *International Symposium on Friction-based Spot Welding Processes*, (International Institute of Welding, GKSS Forschungszentrum, Geesthacht, Germany, 2007), pp. 107–148.
4. Michael Santella et al., "Friction Stir Spot Welding of DP 780 and Hot-Stamp Boron Steels," *Proceedings of Sheet Metal Welding Conference XIII* (American Welding Society, 2008).
5. Michael Santella et al., *Friction Stir Spot Welding of DP 780 and Hot-Stamp Boron Steels*, presented at Sheet Metal Welding

Conference XIII, Livonia, Michigan, May 16, 2008.

6. Y. Hovanski, M. L. Santella, and G. J. Grant, *Friction Stir Spot Welding of Advanced High Strength Steels*, presentation at MS&T, September 2008.

References

1. AWS D8 Committee on Automotive Welding, *Specification for Automotive Weld Quality—Resistance Spot Welding of Steel*, AWS D8.1M:2007 (AWS, Miami, 2007).
2. H. Schmidt, J. Hattel, and J. Wert, “Modelling of the Contact Condition at the Tool/Matrix Interface in Friction Stir Welding,” in H. Cerjak, H. K. D. H. Bhadeshia, and E. Kozeschnik (eds.), *Mathematical Modelling of Weld Phenomena 7*, (Verlag Technischen Universität Graz, 2005), pp. 925–941.
3. Ø. Frigaard, Ø. Grong, and O. T. Midling, *Met. Trans. A*, **32A**, pp. 1189–1200 (2001).
4. P. Reynolds et al., in S. A. David et al. (ed.), *6th International Trends in Welding Research Conference Proceedings*, (ASM International, 2003), pp. 297–301.
5. G. Buffa et al., *Mat. Sci. Eng. A*, **419**, pp. 389–396 (2006).
6. J. E. Gould and Z. Feng, *J. Mat. Proc. Mfg.*, **7**, pp. 185–194 (1998).
7. R. Nandan et al., “Three-dimensional heat and material flow during friction stir welding of mild steel,” *Acta Mat.*, **55**, pp. 883–895 (2007).
8. N. F. Kazakov (ed.), *Diffusion Bonding of Materials*, Pergamon Press, Oxford, U.K. 1985.

D. Friction Stir and Ultrasonic Solid State Joining Magnesium to Steel

Principal Investigator: Glenn J. Grant

Pacific Northwest National Laboratory

902 Battelle Blvd., P.O. Box 999, Richland, WA 99352

(509) 375-6890 ; fax: (509) 376-6034; e-mail: glenn.grant@pnl.gov

Principal Investigator: Yuri Hovanski

Pacific Northwest National Laboratory

902 Battelle Blvd., P.O. Box 999, Richland, WA 99352

(509) 375-3940; fax: (509) 376-6034; e-mail: yuri.hovanski@pnl.gov

Principal Investigator: Michael L. Santella

Oak Ridge National Laboratory

P.O. Box 2008, Oak Ridge, TN 37831-6096

(865) 574-4805; fax: (865) 574-4928; e-mail: santellaml@ornl.gov

Technology Area Development Manager: Joseph A. Carpenter

(202) 586-1022; fax: (202) 586-1600; e-mail: joseph.carpenter@ee.doe.gov

Field Technical Co-Monitors: C. David Warren, Mark Smith

(865) 574-9693; fax: (865) 574-6098; e-mail: warrencd@ornl.gov

(509) 375-4478; fax: (509) 375-4448; e-mail: mark.smith@pnl.gov

Contractors: Oak Ridge National Laboratory (ORNL) & Pacific Northwest National Laboratory (PNNL)

Contract Nos.: DE-AC05-00OR22725 & DE-AC06-76RLO1830, respectively

Objective

- Establish the applied technical understanding necessary to produce robust joints between magnesium alloys and steel using solid state joining (friction stir welding [FSW] and ultrasonics).
- Develop the fundamental relationships influencing bond formation in metallurgical, mechanical and chemical forms created during FSW and ultrasonic welding (USW) solid state processes. Ascertain their responses to changing alloys, product forms and surface conditions as they affect creation of structural joints between magnesium and steel.
- Determine the effect of FSW and ultrasonic joining on corrosion protection coatings and characterize the corrosion performance of joined assemblies.

Approach

- Systematically evaluate the application of friction stir and ultrasonic processes to welding of magnesium to steel. Develop an improved understanding of the interaction of each unique energy source with appropriate alloy/product form combinations.
- Investigate the fundamental aspects of bond formation (metallurgical and/or mechanical) during the solid state process and investigate the response to changing alloys, product forms (wrought, castings) and surface conditions (coatings).
- The materials being joined (magnesium and steel) form a strong galvanic couple. Strategies to prevent corrosion in the joint, including potentially unbroken interlayers or transition materials, complete encapsulation,

coatings or hermetic adhesives that are welded through during the joining process will be employed to mitigate the potential for galvanic coupling.

Accomplishments

- A steering committee was established that includes representatives from the automotive original equipment manufacturers (OEMs) Ford, GM, and Chrysler. This committee will meet by conference call once a month so that project progress and direction can be reviewed.
- Initial project kickoff meeting was held with the OEM steering committee members in the third quarter 2008 to identify issues related to joint geometry, fit-up, processing, etc. for dissimilar material welding. An agreement was reached on applicable alloy forms and gauges.
- Performed literature review in relevant topic areas to provide starting points for process development.
- Developed introductory experimental design parameters for magnesium to steel joints using both friction stir and ultrasonic welding techniques.
- Procured initial materials in several of the applicable alloy forms and gauges to begin testing. Coordinated with the Magnesium Front End Research and Development group to obtain materials in support of dissimilar joining goals.
- Initiated systematic evaluation of applicable joining parameters on several combinations of magnesium and steel in lap configurations.

Future Direction

- Complete preliminary testing of FSW and USW in Mg-steel joints using variations of uncoated and coated steels with AZ31B and AM60 magnesium alloys.
- Perform investigation into bond formation and performance as a function of joining parameters.
- Develop an improved understanding of the interaction of the energy source with appropriate alloy/product form combinations in FSW. Factors affecting joint strength will include tool design, process speed and feed and pin design and location relative to interface.
- Determine the effect of sonotrode tip wear in Mg-steel joints and investigate a limited number of alternative tip materials or process strategies to mitigate wear.

Introduction

Decreasing automobile weight can directly contribute to reducing fuel consumption. Increasing the use of lightweight materials and implementing manufacturing technologies that enable the use of lightweight materials are the two primary paths toward weight reduction. In some situations, lightweight materials can be directly substituted for higher density materials, but there are barriers to direct substitution. In a modern multi-material vehicle, lightweight materials such as aluminum and magnesium alloys can be a challenge to attach to underlying substructure, which is usually composed of steel. Even in aluminum- and magnesium-intensive designs where entire substructures may be constructed of lightweight metals, there remains a need to join

the substructure with other parts of the body-in-white such as the predominantly steel passenger safety cage. Joining methodologies available in the cost environment relevant to automotive manufacturing include resistance spot welding, adhesives, linear fusion welding, hemming, clinching, bolting and riveting. However, because of the highly dissimilar natures of the materials, magnesium/steel joints are extremely problematic. Magnesium-to-steel joints cannot be simply fusion welded due to the extreme differences in their melt temperatures, and joining methods that require a large amount of plastic strain in the magnesium component suffer from magnesium's poor ductility at room temperature.

As alternative joining methodologies, friction stir welding (FSW), friction stir spot welding (FSSW), and ultrasonic welding (USW) may be able to overcome traditional barriers to join and construct hybrid magnesium/steel components. These solid state joining methods provide unique joining capabilities that, if realized, may potentially produce faster and more economical alternatives to current technologies (bolting/riveting). However, FSW and USW for dissimilar magnesium/steel combination are significantly underdeveloped for broad deployment.

The purpose of this project is to develop an applied understanding of the following:

- localized metal forming and potential metallurgical bonding that develops during FSW, FSSW, and USW
- the influence of process parameters on joint strength and performance
- the interaction of both joining processes with existing corrosion protection methods and their corrosion performance.

Approach

While the potential for utilizing solid state joining processes such as FSW and USW to overcome the traditional difficulties associated with joining magnesium to steel is emerging, many challenges remain. Insufficient understanding of the proper processing conditions required to achieve robust joints has hampered any comprehensive evaluation of performance (strength, fatigue, durability, crash performance). Minimal existing research has yet to evaluate feasible joint geometries, and no emphasis on employing the benefits of solid state technologies in mitigating the galvanic corrosion in magnesium/steel joints has been evaluated.

This project is designed to overcome many of these technical barriers by performing three primary tasks. Task 1 will focus on systematically evaluating the application of friction stir and ultrasonic processes to the welding of magnesium to steel in a lap configuration. The work includes developing an improved understanding of the interaction of each unique energy source with appropriate alloy/product form combinations and

is intended to provide a baseline conceptual feasibility for the remaining work.

If Task 1 is completed successfully, Task 2 will concentrate on investigating the fundamental aspects of bond formation (metallurgical and/or mechanical) during the solid state process. This phase of the project will also include an investigation into the response to material variation due to changing alloys, product forms (wrought, castings) and surface conditions (coatings). This task will allow for further investigation of favorable methodologies outlined during the concept feasibility phase with the potential of further increasing joint strength.

Task 3 will focus on investigating strategies to prevent corrosion in the joint. This will include evaluating the effects of potentially unbroken interlayers or transition materials as well as coatings or hermetic adhesives that are welded through during the joining process. These tasks and associated deliverables are intended to enable a broader application of solid state joining technologies while further facilitating the joining of magnesium to steel.

Materials and Experimental Details

As the solid state joining technologies evaluated herein are completely different, unique hardware is being used for the development of each joining process.

Friction Stir Welding

Friction stir technologies will be developed primarily using a high-stiffness precision friction stir welding machine located at PNNL (Figure 1). This machine is capable of maintaining tool runout at less than 0.0004 inch (in.) and can apply vertical process loads in excess of 30 kilo-pounds per square inch (Kip). With the capability of producing welds of 96 in. long and an operating envelope that can accommodate part configurations larger than 48 in. high, this machine provides flexibility in evaluating the various product forms applicable to Mg/steel structures.



Figure 1. Precision FSW machine located at PNNL.

Friction stir joints between magnesium and steel are produced in a lap configuration with the magnesium located on the tool side of the joint. FSW tools are plunged through the thickness of the magnesium to the interface of the two materials and are subsequently translated at depth for a predetermined length. Various techniques have been designed to promote the joining characteristics of the interface, including tools that beneficially disturb the steel surface creating clinch points or rough surfaces for the locally plasticized magnesium to adhere.

Ultrasonic Welding

Research and development in ultrasonic solid state capabilities will take place primarily at ORNL. The research scale ultrasonic test frame shown in Figure 2 is capable of applying up to 2500 Watts (W) at 20 kilo-Hertz (kHz).

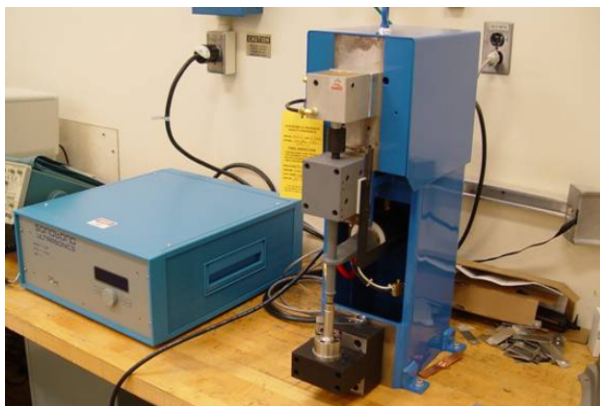


Figure 2. USW machine located at ORNL.

Results

Preliminary ultrasonic welds were made with a Sonobond CLF2500 using a pedestal welding station. The rated conditions at the welding tip on this equipment are 20 kHz frequency with 25 micrometers (µm) amplitude. A variety of on-hand materials are being used for ultrasonic welding trials, while reference materials are being acquired. The magnesium alloys used for the initial welds were 1.6 mm thick AZ31-H24 sheet and 2 mm thick AM60B die castings. Coupons of both alloys were welded to those of 1 mm thick hot-dip galvanized mild steel (MSHDG) to provide specimens for metallographic examination. Optical micrographs of these spot welds are shown in Figures 3 and 4. For this combination of metals, there were no indications of defects or chemical reactions that might compromise weld integrity.

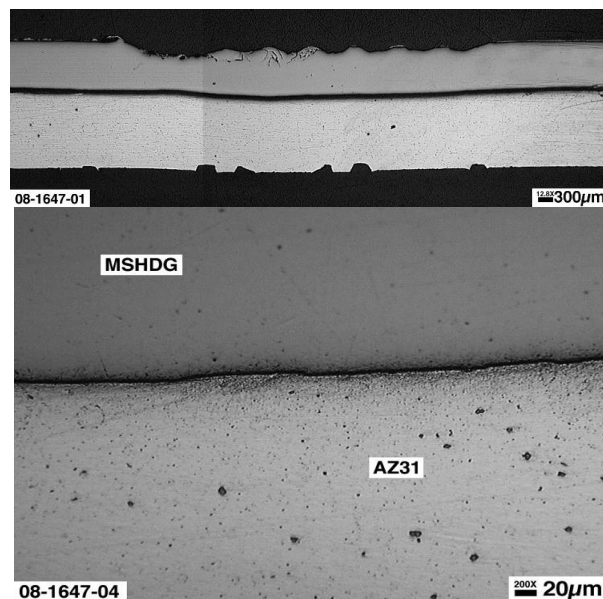


Figure 3. The top micrograph shows the overall view of hot-dip galvanized mild steel ultrasonically spot welded to AZ31; the dark line at the interface is a polishing artifact. The bottom provides detail at the welded interface between the mild steel (MSHDG) and AZ31.

Coupons of AZ31 nominally 25 mm wide x 100 mm long were also welded to mild steel coupons of the same size to produce specimens for lap-shear testing. A 25 mm overlap was used for making lap-welded coupons with spot welds centered in the overlap regions. The lap-welded

specimens were shear tested using a crosshead velocity of 10 mm/min. The specimens were not shimmed in the grips, and no guides were used to constrain specimen rotations during testing. Eleven AZ31-mild steel specimens were tested to arrive at an average lap-shear strength of 2.68 ± 0.41 kiloNewtons (kN).

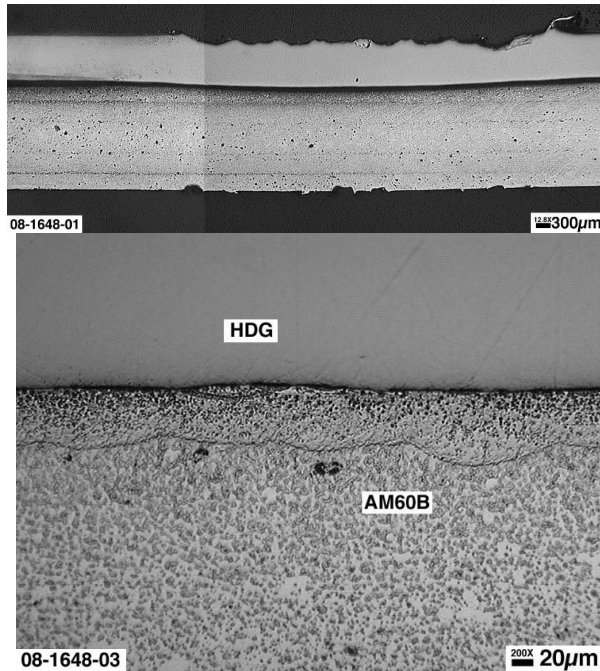


Figure 4. The top micrograph shows the overall view of hot-dip galvanized mild steel ultrasonically spot welded to AM60B; the dark line at interface is a polishing artifact. The bottom provides detail at the welded interface between the mild steel (MSHDG) and AM60B.

Conclusions

The project was initiated in the latter half of 2008, and a kickoff meeting with the principals from PNNL, ORNL, and members from the OEM steering committee took place in the third quarter of 2008. With this late start in 2008, much of the intended initial project scope is still in progress. As one of the initial project goals was to concentrate on alloys and forms corresponding to those used in the Magnesium Front End Research and Development program, some delay was also experienced in attaining corresponding materials.

The project is poised to make rapid progress in the first quarter of 2009 as magnesium materials become available. The initial work on ultrasonic bonding has already shown joint strength above the project's targeted values for Phase 1 of the program, so reaching the later project goals and milestones is considered feasible.

E. Friction Bit Joining—An Innovation in Dissimilar Metal Joining

Principal Investigator: Zhili Feng

Oak Ridge National Laboratory

P.O. Box 2008, Oak Ridge, TN 37831-6095

(865) 576-3797; fax: (865) 574-4928; e-mail: fengz@ornl.gov

Principal Investigator: Michael P. Miles

Brigham Young University

265 CTB, Provo, UT 84602

(801) 422-1858; fax: (801) 422-0490; e-mail: mmiles@byu.edu

Technology Area Development Manager: Joseph A. Carpenter

(202) 586-1022; fax: (202) 586-1600; e-mail: joseph.carpenter@ee.doe.gov

Field Technical Monitor: C. David Warren

(865) 574-9693; fax: (865) 574-6098; e-mail: warrencd@ornl.gov

Contractor: Oak Ridge National Laboratory (ORNL)

Contract No.: DE-AC05-00OR22725

Objective

- Develop the technical basis for and demonstrate the viability of a newly invented solid-state joining process—friction bit joining (FBJ)—for joining dissimilar metals such as aluminum (Al) or magnesium (Mg) alloys and advanced high-strength steels (AHSSs) for use in auto body structures to achieve a balance in cost savings, lightweighting, structural durability, and impact performance.

Approach

- Perform Design of Experiment (DoE) for key process variables that influence the joint strength.
- Characterize bonding interface for better understanding of the basic bonding mechanisms between dissimilar metals.
- Develop process window for different material and gauge combinations.

Accomplishments

- Demonstrated the feasibility of FBJ of dissimilar metals (Mg to steel and Al to steel).
- Achieved metallurgical bonding and relatively low process load.
- Demonstrated initial joint strength exceeded the Phase I target and that of self-piercing rivets.
- Achieved reasonably fast process time (less than 3 s) with good properties.

Future Direction

- Continue DoE evaluation of key process variables that influence joint strength.
- Continue bonding interface characterization and bonding mechanisms investigation.
- Determine feasibility of combining FBJ with adhesive bonding for weld bonding.
- Determine feasibility of FBJ corrosion control and prevention through process innovation and coating.

- Develop mechanized joining-bit feeding system for high-speed, high-volume production.
- Conduct an industry implementation business case analysis for the process.
- Explore and develop a technology-transfer and commercialization partnership.

Introduction

The automotive industry and the U.S. government are aggressively pursuing increased use of lightweight materials such as Mg alloys and Al alloys in auto-body structures for improved vehicle fuel efficiency. Next generation vehicles will require optimum use of a variety of engineering materials, ranging from AHSSs to lightweight materials such as Al and Mg alloys, composites, and other materials, to achieve a balance in cost, lightweighting, durability, and crashworthiness. Use of vastly different lightweight material combinations in body structures presents a number of technical challenges in automotive body-in-white assembly. One of them is joining dissimilar materials to form integrated structural components to meet design and performance requirements [1,2].

Dissimilar metal joining—joining of vastly different materials such as Mg and steel, Mg and Al, and Al and steel—is generally considered to be out of the “comfort zone” of the existing joining and attachment technologies used in high-volume mass production. Conventional fusion welding processes, including gas metal arc welding, laser welding, and resistance spot welding (RSW), are not suitable for welding dissimilar materials because of the metallurgical incompatibility of these materials during melting and solidification. Self-piercing riveting (SPR) is difficult to apply to AHSSs due to the inadequate strength of rivet materials and the equipment limitations. Application of SPR for Mg alloys is also problematic because of their low ductility. Mechanical fastening and adhesive bonding have cost and performance penalties.

This project aims at developing a new solid-state joining process particularly suitable for dissimilar metals. This newly invented process, FBJ, combines the process advantages and overcomes the fundamental shortcomings of the solid-state friction stud welding process and the mechanical SPR process. A proof-of-concept study has

produced surprisingly good results in joining dissimilar materials.

A two-phase, gated programmatic approach has been adopted for this project. This report covers the progress in the first 3 months of a 12-month, Phase I, Concept Feasibility research project that started in June 2008.

Phase I research and development (R&D) focused on further evaluating and identifying the critical factors/variables governing the FBJ process, the process characteristics, and the metallurgical bonding mechanisms between dissimilar metals. More comprehensive R&D will be performed in Phase II (Technical Feasibility) of the project, leading to eventual field demonstration of the FBJ technology. Phase II will also include identifying potential commercial partners and eventual partnership with technology-transfer and commercialization candidates.

The Department of Energy’s FreedomCAR and Vehicle Technologies Lightweighting Materials thrust and the National Science Foundation’s Materials Processing and Manufacturing Technology Program cosponsored the Phase I effort, which is being carried out jointly by ORNL and Brigham Young University.

Process Principle of FBJ

FBJ creates a metallurgically bonded spot joint in two or more sheets of the same metal or dissimilar metals by a combination of the cutting and friction bonding action of a high-strength consumable joining bit. The essence of the FBJ process is illustrated in Figure 1. FBJ comprises two essential phases. It starts with an initial cutting phase where the top layer (or layers) is penetrated by the rotating joining bit under applied axial load. The process then transitions to the frictional-joining phase in which the rotating bit and surrounding sheet materials are frictionally heated to a high temperature to facilitate material flow and bonding. In a manner similar to friction stud

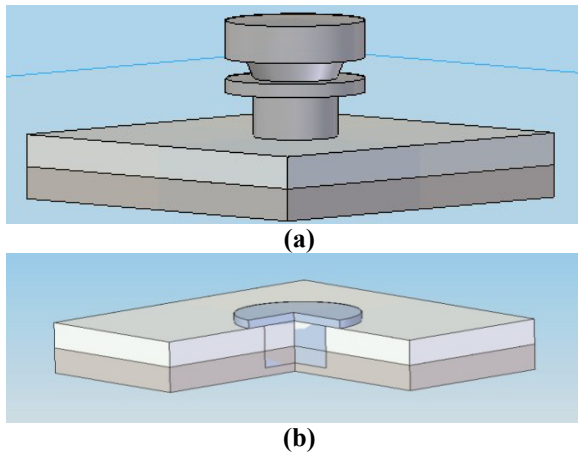


Figure 1. Schematic representation of FBJ process. The operation begins with cutting through the top layer of material, shown in (a). The rotational speed of the bit is then increased to generate frictional heating and material flow to join the sheets. At the end, the top part of the bit held by the machine is self-separated from the bottom, bonded to the workpiece, leaving a relatively smooth joint, as seen in (b).

welding, at the end of the operation a metallurgical bond is formed between the joining bit and the different sheet materials as a result of diffusion across the interface of different metals under high temperature and high pressure. The joining bit is consumable—it is left in the workpiece and forms an integral part of the weld.

FBJ incorporates a unique self-break-off feature by means of special machine spindle design and simple joining bit geometry design. The part of the joining bit bonded to the workpiece is automatically sheared off from that in the machine holder at the end of the operation, leaving a relatively smooth joint surface above the bit flange, as shown in Figure 1. The unique self-break-off feature makes it possible to automate the process in a high-speed production environment and eliminate the need for the after-welding cutting operation. FBJ is fast: the total process time in the concept feasibility study ranged from 2 to 5 seconds.

A prototype machine, shown in Figure 2, was designed and built for FBJ during Phase I. The C-frame support configuration is very similar to that commonly used in robotic RSW machines on body assembly lines. As shown in the figure, the C-frame in this first prototype machine is quite



Figure 2. Prototype FBJ machine with a C-frame.

bulky. However, the surprisingly low axial loads obtained in the welding trials (ranging from 8 kN to 12 kN) indicate that the size of the C-frame can be greatly reduced in future production systems.

Progress in FY 2008

Experiments were carried out on two material combinations: 1.4-mm-thick uncoated dual phase (DP) 980 steel welded to 1.8-mm-thick Al alloy 5754 (AA 5754) and 1.4-mm-thick uncoated DP 980 welded to 1.8-mm-thick Mg alloy AZ91. Figure 3 shows an example of FBJ spot welds made between AA 5754 and DP 980. The weld cross-section and bonding interfaces are shown in Figure 4 and Figure 5,



Figure 3. Appearance of FBJ between DP 980 and AA 5754.

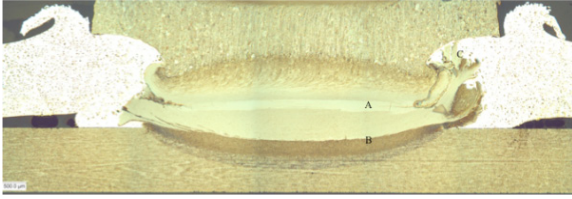


Figure 4. Cross section of FBJ composed of AA 5754 (top sheet), DP 980 (bottom sheet), and 4140 steel joining bit (center).

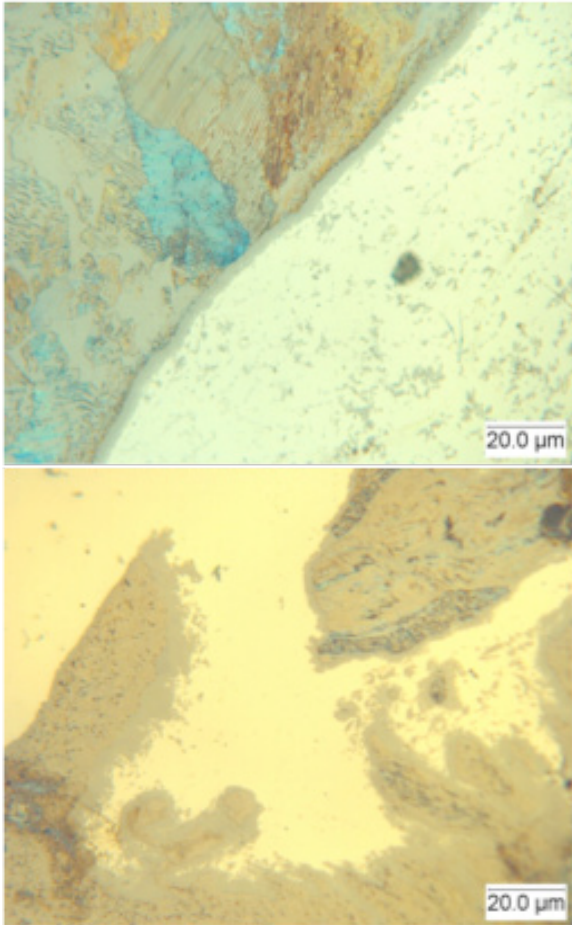


Figure 5. Bonding interface between AA 5754 and DP 980. Metallurgical bonding is evident.

respectively. Clearly, metallurgical bonding has been achieved between DP 980 steel and AA 5754. Metallurgical bonding was also achieved between DP 980 steel and Mg alloy AZ91.

A series of experiments was carried out to determine the effects of different process variables on lap-shear failure load. Table 1 shows the parameter variables that had the most influence on

Table 1. Joining parameters with the greatest influence on lap-shear failure loads

Bit length (mm)	Joining plunge rate (mm/min)	Depth of plunge (mm)
4.4	36	2.8
6	66	3.3

the lap-shear tensile strength for the DP 980-AA 5754 material combination. The shading indicates the process conditions that resulted in the best lap-shear strength—reaching an average of 6.5 kN from three replicate specimens.

In the feasibility welding trials conducted so far with Mg alloy, the lap-shear strength for Mg alloy AZ91-DP 980 steel dissimilar welds ranged from 3.0 to 4.8 kN.

The joint strengths of dissimilar FBJ welds are very encouraging. Both Mg-steel and Al-steel FBJ welds far exceed the 1 kN feasibility target strength for Mg-steel and Al-steel joining set forth by the U.S. Automotive Materials Partnership (USAMP).

Sun et al. [3] reported SPR experiments performed on combinations of high-strength, low-alloy (HSLA) 350 steel and AA 5754. Their results were used to benchmark the FBJ results obtained so far in this study. Although the steels used in the two studies were different (DP 980 vs HSLA 350), the weaker material (AA 5754) was the same in both studies and provided the basis for comparison. To effectively compare FBJ and SPR, the bond areas must be known because bond area affects the strength of the joint. The bond area for the FBJ joints was determined by optical measurement of the fracture surface across two diameters of the weld, 90° apart. For SPR, the effective bond area was estimated by considering the rivet geometry, material thickness, and failure mode (rivet-head pullout or a rivet-tail pullout) [3]. SPR results for a joint composed of 1.6-mm HSLA 350 and 2.0-mm AA 5754-O can be found in reference [3]. These material thicknesses are slightly greater than the joints presented in this paper, but as stated before, the weaker materials are the same alloy of similar gauge, so joint

strengths were compared using bond areas. The bond area for the FBJ joints was 28 mm² and for the SPR joints 47 mm². Lap-shear failure loads were 6.3–6.5 kN for FBJ and about 5.2 kN for SPR. Based on these results, the FBJ joint supports a much greater load per unit bond area than the SPR joint by a factor of 2.

Figure 6 shows the failure mode of FBJ in lap-shear tensile tests. For both steel-Al and steel-Mg joints, it was possible to demonstrate a weld-button-pullout failure mode in which the steel joining bit remained joined to the steel sheet and the Al or Mg sheet was separated from the joining bit. This failure mode is typically associated with high failure strength.



Figure 6. Weld button pullout failure mode observed in FBJ of AA 5754 to DP 980.

Future Direction

The focus of R&D activities in FY 2009 will be on completing the following tasks.

- **DoE Evaluation of Process Conditions.** DoE studies will be conducted to further

identify the key process variables influencing the strength of FBJ joints.

- **Microstructure Characterization of the Bonding Interface.** Different microstructural and compositional analysis techniques will be used to study and understand the bonding interface to elucidate the bonding mechanisms between the dissimilar metals.
- **Feasibility of Combining FBJ with Adhesive Bonding.** Initial trials will be on steels to Al alloys.
- **Feasibility of Corrosion Prevention of FBJ.** Various coatings as well as process innovations will be explored for corrosion prevention and control.

Presentations/Publications/Patents

1. M. Miles et al., “Friction Bit Joining of Dissimilar Material Combinations of High Strength Steel DP 980 and Al Alloy AA 5754,” *SEA 2009 World Congress*, Detroit, Michigan, Paper No 09M-0232.
2. M. Miles and Z. Feng, “Spot Joining of Dissimilar Combinations of Steel and Light Metals Using a New Consumable Bit Technology,” (Invited) *Joining Dissimilar Metals Conference II*, American Welding Society, March 3–4, 2009, Orlando, Florida.

Acknowledgements

We would like to acknowledge the contributions of the following individuals and organizations.

Industry Advisory Committee:

- Chrysler: W. Marttila
- Ford: W. Charron, E. Hetrick
- GM: J. Quinn, J. Fickes, D. Hutchinson

USAMP Metals Joining Team

USAMP Multiple Materials Vehicle Team

Auto/Steel Partnership Joining Technologies Team

USAMP Manufacturing Team

References

1. J. F. Quinn, "Joining Challenges in the Automotive Industry," ORNL Materials Joining Advisory Committee Meeting, November 2, 2007, Oak Ridge National Laboratory, Oak Ridge, Tennessee.
2. *HYBRIDMAT 2: Strategies in the Joining of Hybrid Materials in Automotive Structures—a Mission to France and Germany, May 2004*. Global Watch Mission Report (UK Department of Trade and Industry Global Watch Service, September 2004).
3. X. Sun and M. A. Khaleel, "Strength estimation of self-piercing rivets using lower bound limit load analysis," *Science and Technology of Welding and Joining*, **10**(5), pp. 624–625 (2005).

F. Weld Element and Joining Process Technology Development

Principal Investigator: Douglas J. Bammann
 Professor, Mechanical Engineering
 Mississippi State University
 210 Carpenter Bldg.
 Mississippi State, MS 39762
 (662) 325-3260; e-mail: djb215@me.msstate.edu

Co-Principal Investigator: Sergio Felicelli
 Associate Professor, Mechanical Engineering
 Mississippi State University
 210 Carpenter Bldg.
 Mississippi State, MS 39762
 (662) 325-1201; e-mail: felicelli@me.msstate.e

Postdoctoral Associate: Liang Wang
 Center for Advanced Vehicular Systems, CAVS 2182-B
 Mississippi State University
 Mississippi State, MS 39762-5405
 (662) 325-9235; e-mail: liangw@cavs.msstate.edu

Co-Principal Investigator: Ted Belyteschko
 Walter P. Murphy Professor and McCormick Professor
 Departments of Civil and Mechanical Engineering
 Northwestern University
 2145 Sheridan Road
 Evanston, Illinois 60208-3111
 (847) 491-7270; fax: (847) 491-3915; e-mail: tedbelytschko@northwestern.edu

Co-Principal Investigator: Wing Kam Liu
 Walter P. Murphy Professor
 Director of the NSF Summer Institute on Nano Mechanics, and Materials
 Department of Mechanical Engineering
 Northwestern University
 2145 Sheridan Road
 Evanston, Illinois 60208-3111
 (847) 491-7094; fax: (847) 491-3915; e-mail: w-liu@northwestern.edu

Contractor: Mississippi State University (MSST)
 Contract No.: 4000054701

Objective

- Develop the next generation of weld element and joining process technology (i.e., spot welding) and assess the applicability of new technology for impact simulations and process optimization using lightweight alloys.

Approach

- Currently, weld element performance and failure are based on a simple beam model in which the weld is modeled as a single element between two welded sheets, and failure is postulated to occur when the tension or a moment exceed a certain specified threshold. This type of model does not reflect the thermomechanical details

of the welding process and consequently is unable to address variations in strength due to differences in weld process parameters and the metallurgy of the materials being joined.

- To develop the next generation of weld analysis technology in which details of the welding process and the metallurgy of the parent material are reflected in the behavior of the weld element, the physics of the resistance welding process must be modeled in detail. The nature of the solidification process within the weld will be studied. The computed thermal history induced during the welding process will be used to predict microstructural evolution within the weld and adjacent material, thereby allowing prediction of the large mechanical property gradients associated with the weld. The evolution of damage in the weld under subsequent high strain rate loading will be studied with strain rate dependent constitutive models.
- The development of the resistance spot welding process has remained largely empirical because the process is extremely complex due to friction-induced deformation and heat generation. We plan to assess the feasibility of developing a weld element technology and a three-dimensional (3D) process model which will enable better design of the spot welding process.

Accomplishments

- Developed thermoelectrical and thermomechanical models with ABAQUS to predict temperature distribution and residual stress during the spot welding process.
- Developed a two-phase Bammann-Chiesa-Johnson (BCJ) model, and implemented the UMAT for this model in ABAQUS.
- Developed a multiscale fracture model to apply the multiresolution continuum theory to formation and propagation of adiabatic submicro-, micro-, and macro-shear bands resulting from microstructure damage, growth, and coalescence, which eventually form submicro-, micro-, and macro-cracks in steel alloys.

Future Direction

- Compare the results from ABAQUS with Sysweld results.
- Perform an experimental study for spot welding, including investigating the effects of process parameters on the nugget size and residual stress. The experimental data will be used to validate the thermoelectrical and thermomechanical models.
- Use Gleeble simulator to simulate the welding process and obtain the material constants for BCJ model for low carbon steel AISI 1018.
- Integrate the thermoelectrical and thermomechanical models with UMAT (two phase BCJ model) to predict the stress-strain curve with different process parameters (current, pressure, and weld time).

Introduction

Resistance spot welding is a common joining process used in automotive manufacturing, with thousands of spot welds in a single vehicle. To realistically simulate the behavior of a vehicle under crash conditions, the mechanical behavior of spot welds under dynamic loading must be incorporated [1–2]. Currently, spot welds are simulated using general shell elements for each sheet of a spot-welded joint and a single bar element for each spot weld, which connects the two sheets of a joint at two nodal joints [3–4]. This approximation is very rough and causes an unreliable evaluation of the stiffness around the spot weld [5].

Other techniques [6] make use of a 3D nugget connected to the shell elements. But in this case a good approximation of the stresses is achieved only through a considerable refinement of the mesh next to the spot. As a result, this modeling procedure is not very practical when several spot welds are present. Knowledge of the stress field surrounding spot welds requires an accurate modeling of the entire structure. Salvini et al. [5] proposed a new finite element (FE) assembly to account for the structural behavior of the region surrounding a spot weld. The assembled elements, connected by a link, form the spot weld connection between two metal sheets. Zhang and

Taylor [7] proposed a so-called umbrella model to account for the radial stresses around a spot weld for stiffness analysis and fatigue prediction for different types of spot-welded structures. A recent review on the subject of different FE models of spot welds for various types of analysis has been published by Palmonella et al. [8].

A next generation spot weld element is needed in which details of the welding process and the metallurgy of the parent material are reflected. In this report, an FE model was developed to predict the process-property relations in the resistance spot welding, which will be implemented in the spot weld element formulation.

Mathematical Model with ABAQUS

Advantages of ABAQUS

To obtain more accurate predictions of the final mechanical properties of spot welds than those produced using SYSWELD, a similar FE model was developed using a commercial FE analysis package, ABAQUS. Using ABAQUS to simulate spot welding process has several key advantages.

- Allows for use of user-defined internal state variable (ISV) models to calculate residual stress and material phase distributions.
- Includes mechanical aspects of spot welding process (applied electrode force) through coupled thermomechanical analysis package—affects residual stresses and contact resistances.
- Allows for use of kinetically based calculations for phase transformation.

The BCJ ISV model is used to model the residual stress resulting from the mechanical loading of the workpieces and the thermal expansion due to heating and accounts for differences in mechanical response among phases present in material. The BCJ model includes the interface stresses, transformation induced plasticity that occur in multiphase materials, improving the accuracy of residual stress calculations. This model also predicts the change in phase volume fraction throughout the welding process using a physically based kinetic phase transformation model, a more accurate method than the empirically based

approach adopted by SYSWELD. More accurate predictions of the residual stresses and phase distributions lead to more accurate predictions of mechanical properties for spot welds.

Model Structure

To model the complex coupling of thermal, electrical, mechanical, and metallurgical processes occurring in the spot welding process, the integration scheme shown in Figure 1 was developed to pass output data between the coupled thermomechanical and thermoelectrical packages already available in ABAQUS.

The steps laid out in Figure 1 represent all thermal, electrical, and mechanical aspects of the actual spot welding process, where the initial mechanical loading transmitted through the electrodes is represented by a purely mechanical analysis. The deformation resulting from this step is then passed into a thermal-electrical analysis, representing electrical loading of the weld assembly, where a current load is applied via the electrodes. The resulting temperature field generated by the heating is passed into a coupled thermal-mechanical analysis to capture the temperature-dependency of the deformation, after which the newly deformed geometry is passed back to the thermal-electrical analysis. The thermal-electrical and thermal-mechanical analyses proceed to update one another at small time steps ($\theta \sim 10^{-6}$ sec) until some specified total time is achieved. At this point the geometry and temperature field are exported to a final coupled thermal-mechanical analysis to calculate final values of temperature and geometry, as well as residual stress and phase distribution via the BCJ model. The final state of the spot weld is then made available through analysis of the final stress state of the weld, temperature distribution, phase distribution, and nugget size.

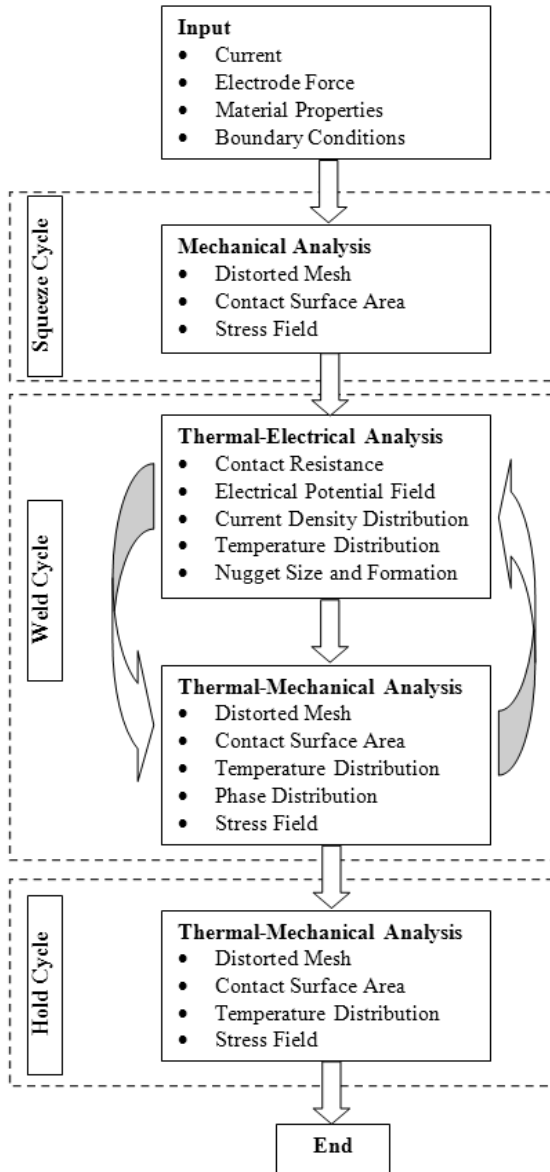


Figure 1. Integration scheme for ABAQUS spot welding procedure.

The nugget size and phase distribution may be validated experimentally through metallographic techniques and microindentation on test specimens made under different loading conditions. The accuracy of the final stress state in the weld may be tested by comparing simulated and experimental stress vs strain response for cases of tensile loading.

Temperature and Strain Rate Dependent Test Using Gleeble Thermomechanical Simulator

The goal of this test is to obtain material constants for a constitutive model (BCJ model developed by Doug Bammann) for steel alloys that contains phases such as martensite and austenite phases for AISI 1018 low carbon steel material. This BCJ model will be able to predict stress-strain relationships of steel alloys under high temperature processing conditions where phases are evolved with temperature and deformation.

Test Matrix

At least two strain rates (S1, S2) and two temperature settings (T1, T2) are required for tension, compression, and reverse loading tests for each phase. The tested coupon samples will be heated through a thermal cycle such that phases will be in solution and a single phase will be precipitated with control thermal cycles. Once the coupon sample is close to 100% of a particular phase, testing will be conducted to collect stress-strain-strain rate responses. The constitutive BCJ model will then be correlated with those responses measured from a Gleeble machine.

Multiscale Fracture Simulator

This work was performed by Wing Kam Liu, Rong Tian and Ted Belytschko (Northwestern University) and Leveraged by the Dynamic Microstructure Design Consortium (ONR Contract: N00014-05-C-0241), under a program titled Microstructure-Property Relations, Multiresolution continuum simulation and its Applications to damage, adiabatic shear band, and fracture failure.

In the past 12 months, the numerical simulation work focused on application of the multiresolution continuum theory to formation and propagation of adiabatic submicro-, micro- and macro-shear bands resulting from microstructure damage, growth, and coalescence, which eventually form submicro-, micro- and macro-cracks in a steel alloy. The multiresolution continuum theory has been extended to three dimensions, and a 3D parallel multiresolution code has been developed. Further improvement is needed.

In multiscale materials, permanent deformation is accompanied by energy dissipation at several distinct scales. This materials system also

undergoes inhomogeneous deformation at more than one length scale during damage initiation, growth, and final failure. Furthermore, during the extreme high strain rates, large strains, high temperatures, and high pressures dynamic loading of the microstructured materials system, thermal diffusion also affects the scale of the resulting nested adiabatic shear band (ASB) multiscale fracture.

This research seeks to develop a probabilistic microstructural continuum theory (PMCT) for the nested multiresolution ASB assisted fracture. The goal is to achieve fundamental understanding of the strength, toughness, damage initiation and progression, and multiscale failure of microstructural material systems under extreme loading conditions. In addition, the proposed PMCT can also be used in innovative materials design and fabrication of materials and structures that absorb energy, deflect penetrators, and/or laterally disperse momentum.

As shown in Figure 2, the proposed theory begins with a prototype material sample. We use advanced experimental and imaging techniques to create the digital data sets for material microstructure. The microstructure evolution can be mapped at multiple scales. A rigorous mechanical-science framework for multiscale modeling is being developed to predict macroscale properties accurately based on microstructure descriptions without resorting to empiricism. This framework is constructed based on a statistical inference theory where validation and model uncertainty quantification are done by combining both high fidelity stochastic simulations and limited physical experimental data.

For the first time, we have developed a multiresolution 3D simulation of the fracture process zone model with the aid of advanced experimental techniques that rapidly reconstruct the 3D microstructures and computational science as shown in Figure 3. Figure 3 depicts the macroscale and microscale experiments providing the crack opening displacement (COD) versus the applied load and the microstructures within the multiscale fracture process zone. Using high performance computing, a 3D microstructure simulation reveals the microstructure evolutions

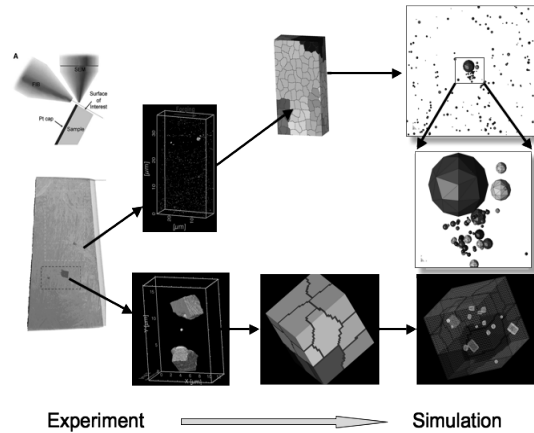


Figure 2. Focused ion beam/scanning electron microscopy experiments and imaging data to multiresolution analysis.

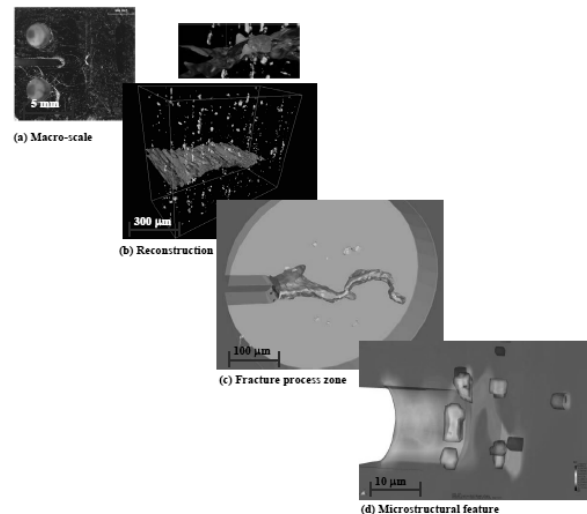


Figure 3. Three-dimensional microstructure reconstructions and simulations of fracture process zone. (a) and (b) show the crack tip specimen and microstructure reconstruction providing the microstructures within the fracture process zone and COD versus the applied load, respectively. Using high performance computing, a 3D microstructure simulation [(c), (d)] reveals clearly the microstructural features and interplay during the development of the fracture process zone and provides a deeper understanding of the effects of microstructures on materials properties.

and the effects of microstructures on materials properties. The combination of the 3D microstructure data sets and the 3D large-scale simulations provides a unique opportunity in developing a comprehensive understanding of

microstructure-property relationships to systematically design materials and structures with specific desired properties.

While materials science and experimental observation can heavily influence the model, it is ultimately mathematical theory that will unify these ideas. We envision that the science based mathematical foundation starts with linking spatial scales for continuous resolution of a microstructure. We aim to zoom into a microstructure in the same way that modern satellite technology allows us to zoom into images anywhere, anytime, and with any resolution. Hence, the separation of data by scales is done through the use of computer imaging and materials science knowledge. The quantification of nanostructured and microstructured data sets is performed through the use of statistical, complexity, and decision making theories, whereas the scale linking is done via testing and characterization of the data set samples.

To establish the validity of our models for these very heterogeneous microstructure evolutions subject to extreme environments, we are making comparisons with data on known materials subjected to mechanical, thermal, and chemical diffusion environments. We then use multiscale physics to design better multifunctional materials and use the above refined multiresolution data sets to develop a technique to extract the missing information that would otherwise remain hidden in the results of the carefully designed experiments. A good start is to link the missing science with existing single scale models by introducing microstructure fluxes, identifying microstructure transition events, and linking scales by introducing microstructure couple fluxes. In this context, models of random media can be efficiently used to derive an estimation of the macroscopic behavior of a physical system from the knowledge of the microscopic behaviors of its constituents.

Conclusions

Thermoelectrical and thermomechanical models were implemented in ABAQUS. The BCJ two-phase model was developed and implemented into

ABAQUS as UMAT. The Gleeble simulator will be used to obtain the BCJ model constants. Spot welding experiments will be performed to validate the thermoelectrical and thermomechanical models.

Presentations/Publications/Patents

None.

References

1. S. D. Sheppard and M. Strange, "Fatigue Life Estimation in Resistance Spot Welds: Initiation and Early Growth Phase," *Fatigue & Fracture Engineering Materials & Structures*, **15**(6), pp. 531–549 (1992).
2. X. Deng, W. Chen, and G. Shi, "Three-dimensional Finite Element Analysis of the Mechanical Behavior of Spot Welds," *Finite Elements in Analysis and Design*, **35**, pp. 17–39 (2000).
3. S. Xu and X. Deng, "An Evaluation of Simplified Finite Element Models for Spot-welded Joints," *Finite Elements in Analysis and Design*, **40**, pp. 1175–1194 (2004).
4. W. Chen and X. Deng, "Performance of Shell Elements in Modeling Spot-welded Joints," *Finite Elements in Analysis and Design*, **35**, pp. 41–57 (2000).
5. P. Salvini, F. Vivio, and V. Vullo, "A Spot Weld Finite Element for Structural Modeling," *International Journal of Fatigue*, **22**, pp. 645–656 (2000).
6. D. Radaj, "Local Fatigue Strength Characteristic Values for Spot Welded Joints," *Engineering Fracture Mechanics*, **37**(1), pp. 245–250 (1990).
7. Y. Zhang and D. Taylor, "Optimization of Spot-welded Structures," *Finite Elements in Analysis and Design*, **37**, pp. 1013–1022 (2001).
8. M. Palmonella et al., "Finite Element Models of Spot Welds in Structural Dynamics: Review and Updating," *Computers and Structures*, **83**, pp. 648–661 (2005).